



universität  
wien

# DIPLOMARBEIT

Titel der Diplomarbeit

Quantifying radioxenon gas releases from a  
TRIGA research reactor

angestrebter akademischer Grad

Magister der Naturwissenschaften (Mag. rer. nat.)

Verfasserin / Verfasser:	Michael LECHERMANN
Matrikel-Nummer:	0135101
Studienrichtung (lt. Studienblatt):	Diplomstudium Physik 411
Betreuerin / Betreuer:	Prof. Dr. Helmuth BÖCK

Wien, im Februar 2010

---



## Kurzfassung

Zur Unterstützung des Kernwaffenteststopp-Vertrages (CTBT) befindet sich ein internationales Kontrollsystem (IMS) im Aufbau, das der Erfassung und Lokalisierung geheimer nuklearer Explosionen dienen wird, sobald der Vertrag in Kraft tritt. Neben Seismik, Hydroakustik und Infraschall wird eine Überwachung von radioaktiven Partikeln und Edelgasen Anwendung finden.

Edelgase sind von besonderer Bedeutung für die Identifizierung unterirdischer nuklearer Explosionen, da es äußerst schwierig für einen Vertragsverletzer wäre, diese daran zu hindern in die Atmosphäre einzudringen. Die Radioxenon-isotope  $^{131m}\text{Xe}$ ,  $^{133m}\text{Xe}$ ,  $^{133}\text{Xe}$  und  $^{135}\text{Xe}$  werden bei Kernspaltung in genügenden Mengen erzeugt und erfüllen erwiesenermaßen die Anforderungen des IMS. Deshalb wurden sie als CTBT-relevant eingestuft und für eine kontinuierliche Überwachung ausgewählt. In letzter Zeit wurden Studien über die Radioxenonabgabe aus Kernkraftwerken und Produktionsanlagen von Radiopharmazeutika veröffentlicht, die Radioxenonabgabe von Versuchsreaktoren wurde jedoch noch nicht untersucht.

Diese Arbeit präsentiert eine erste Quantifizierung des Ausstoßes der vier CTBT-relevanten Radioxenon-isotope eines TRIGA Versuchsreaktors. Zu diesem Zweck wurde ein mobiler Sampler des Swedish Automatic Unit for Noble gas Acquisition (SAUNA) an das Atominstitut Wien gebracht und auf der Reaktorplattform des TRIGA Mark II Reaktors aufgebaut. Luftproben wurden über dem Reaktorbecken und aus den mit Luft gefüllten Bestrahlungsrohren genommen und an das Labor des Swedish Defence Research Agency (FOI) geschickt, wo sie mittels Beta-Gamma-Koinzidenz ausgewertet wurden. Außerdem wurde die Radioxenonabgabe von hoch angereichertem Uran (93% HEU) während der Bestrahlung in einem Bestrahlungsrohr untersucht.

Die vier CTBT-relevanten Xenon-isotope  $^{131m}\text{Xe}$ ,  $^{133m}\text{Xe}$ ,  $^{133}\text{Xe}$  und  $^{135}\text{Xe}$  konnten mit Aktivitätskonzentrationen von 0.01 bis  $1.6 \times 10^4$  Bq/m<sup>3</sup> nachgewiesen werden. Darüber hinaus wurde  $^{125}\text{Xe}$ , das durch Neutroneneinfang von  $^{124}\text{Xe}$  entsteht, in mehreren Proben gefunden. Sein Anteil gegenüber den oben erwähnten Radioxenon-isotopen konnte durch numerische Berechnungen bestätigt werden.

## Abstract

In support of the Comprehensive Nuclear-Test-Ban Treaty (CTBT) an International Monitoring System (IMS) is being established that will be used to detect and locate clandestine nuclear explosions once the treaty has come into force. Besides seismic, hydroacoustic and infrasound techniques the verification regime will employ monitoring of radioactive particulates and noble gases.

Noble gases are of especial importance to identify underground nuclear explosions, since they are most difficult to prevent from migrating into the atmosphere for a treaty violator. The radioxenon isotopes  $^{131m}\text{Xe}$ ,  $^{133m}\text{Xe}$ ,  $^{133}\text{Xe}$  and  $^{135}\text{Xe}$  are sufficiently produced in fission and were proven to fulfill the demands of the IMS. Therefore, they have been classified as CTBT-relevant and selected for continuous monitoring. Recently, studies have been published regarding releases of radioxenons from radiopharmaceutical facilities and nuclear power plants. The radioxenon releases from research reactors, however, have not been studied yet.

This work presents a first quantification of releases of the four CTBT-relevant radioxenon isotopes from a TRIGA research reactor. For this purpose a portable field sampler of the Swedish Automatic Unit for Noble gas Acquisition (SAUNA) was shipped to the Atominstitut of Vienna and assembled on the reactor platform of the TRIGA Mark II reactor. Air samples were taken above the reactor pool and from irradiation tubes containing air and shipped to the lab of the Swedish Defence Research Agency (FOI) for analysis using beta-gamma coincidence techniques. Furthermore, radioxenon releases of irradiated highly enriched uranium (93% HEU) were studied separately.

The four CTBT-relevant xenon isotopes  $^{131m}\text{Xe}$ ,  $^{133m}\text{Xe}$ ,  $^{133}\text{Xe}$  and  $^{135}\text{Xe}$  have been detected with activity concentrations between 0.01 to  $1.6 \times 10^4$  Bq/m<sup>3</sup>. Furthermore  $^{125}\text{Xe}$ , formed by neutron capture of  $^{124}\text{Xe}$  in air, was determined to be present in several samples. Its ratio compared to the above mentioned radioxenon isotopes was conform to numerical predictions.



# Contents

<b>1</b>	<b>Introduction</b>	<b>5</b>
1.1	Nuclear fission and fission products . . . . .	5
1.2	Nuclear weapons . . . . .	7
1.2.1	General . . . . .	7
1.2.2	Types . . . . .	7
1.2.3	Nuclear weapons testing . . . . .	12
1.3	The CTBT . . . . .	16
1.4	Sources of radioxenon . . . . .	19
1.4.1	General . . . . .	19
1.4.2	Civil sources . . . . .	20
1.4.3	Releases from nuclear tests . . . . .	21
1.5	Environmental radioxenon background . . . . .	23
<b>2</b>	<b>Scope of work</b>	<b>26</b>
<b>3</b>	<b>Theory</b>	<b>27</b>
3.1	Characteristics of the four xenon isotopes of interest . . . . .	27
3.1.1	General . . . . .	27
3.1.2	$^{131m}\text{Xe}$ . . . . .	28
3.1.3	$^{133m}\text{Xe}$ . . . . .	29
3.1.4	$^{133}\text{Xe}$ . . . . .	29
3.1.5	$^{135}\text{Xe}$ . . . . .	30
3.2	The SAUNA noble gas measuring system . . . . .	30
3.2.1	General . . . . .	30

3.2.2	The mobile SAUNA OSI field sampler . . . . .	31
3.2.3	The SAUNA lab system . . . . .	32
3.2.4	Detector calibration . . . . .	34
3.3	The TRIGA Mark II reactor . . . . .	38
3.3.1	Design and physical properties . . . . .	38
3.3.2	Fuel inventory and estimated radioxenon emissions . . .	40
3.3.3	Transport of xenon through the reactor . . . . .	41
3.4	The analysis procedure . . . . .	42
3.4.1	General . . . . .	42
3.4.2	The Net Count Calculation (NCC) method . . . . .	42
3.4.3	Calculation of the Minimum Detectable Concentration .	49
3.4.4	Corrections and revisions . . . . .	52
3.5	Classification of radioxenon samples . . . . .	53
<b>4</b>	<b>The measurement campaigns at the TRIGA reactor in Vienna</b>	<b>56</b>
4.1	Experimental schedule and setup . . . . .	56
4.2	Processing and analysis of the samples . . . . .	60
4.2.1	First experimental campaign . . . . .	60
4.2.2	Second experimental campaign . . . . .	61
4.3	Results and discussions . . . . .	63
<b>5</b>	<b>Conclusions and outlook</b>	<b>69</b>
<b>6</b>	<b>Epilogue</b>	<b>71</b>
	<b>Bibliography</b>	<b>72</b>

# 1 Introduction

## 1.1 Nuclear fission and fission products

Nuclear fission is probably one of the most far-reaching discoveries in natural science. Otto Hahn and Fritz Straßmann observed the first induced nuclear fission of uranium in 1938. But it was Lise Meitner together with her nephew Otto Frisch who first suggested nuclear fission as the reason for the detection of  $^{141}\text{Ba}$ , a typical fission product that does not occur in nature [Meitner and Frisch, 1939].

Ever since, an enormous spectrum of technologies has been developed to take advantage out of this process. The energy set free during fission of heavy elements like e.g.  $^{235}\text{U}$  is being used in power plants but also in nuclear weapons. Besides lighter nuclei and energy, fission often produces free neutrons. Although neutrons possess an electric dipole moment, they are uncharged particles. Thus they can easily overcome the electronic shell of an atom and attach to the nucleus. This way, they can induce new fission reactions. In a nuclear reactor this chain reaction is controlled, whereas in a nuclear explosion it is intended to create an uncontrolled chain reaction within the explosive material. In nuclear weapon design much effort is spent to keep this chain reaction going as long as possible, so that preferably much fissile material is used.

Every fission leaves fission products behind, lighter nuclei often times rich in neutrons and radioactive. The amount, in which the fission products are statistically produced, is referred to as fission yield and is normally stated as percentage per fission. It is energetically favorable for the nucleus to split into two parts of different sizes. The yield function drawn against the mass number is

asymmetric and bimodal. Its exact form depends on the neutron energy, as can be seen in figure 1.1. The maxima of the curve lies between the mass numbers 90 and 105 respectively 130 and 140 (amu). Radioxenon isotopes, like  $^{133}\text{Xe}$ , are produced in fairly large quantity during fission.

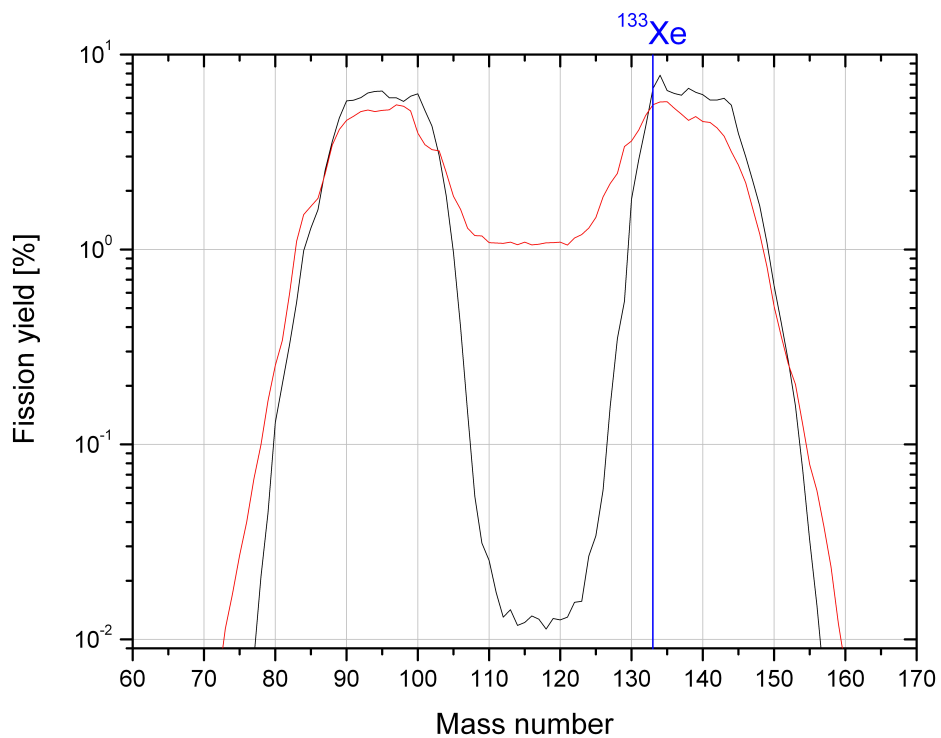


Figure 1.1: Nuclear fission yield for  $^{235}\text{U}$  for fission induced by thermal neutrons (0.025 eV; black line) and high energy neutrons (14.7 MeV; red line) [England and Rider, 1994]

Many fission products do not occur in nature, so a detection of such isotopes represents a firm sign that nuclear fission took place. The isotopic signatures

set free by any nuclear source depend on the distribution of isotopes produced by fission and the activation build-up.

## **1.2 Nuclear weapons**

### **1.2.1 General**

A nuclear weapon is a device that uses nuclear fission or nuclear fusion for its destructive power. Compared to conventional explosives, the quantity of energy released from a nuclear weapon is by far higher. Even with a small yield nuclear explosives can annihilate a whole city within a second and are therefore considered to be weapons of mass destruction. In history only two nuclear weapons have been used offensively, both at the end of World War II. The nuclear bombing of Hiroshima and Nagasaki are estimated to have killed as many as 64,000 people in Hiroshima and 39,000 in Nagasaki within four months after the attacks [Oughterson and Shields, 1956]. Long term effects of ionizing radiation caused even more deaths and illnesses due to damages of genetic material. The vast power of nuclear bombs can be seen in Figure 1.2. Since their infamous debut, the use, development and the control of nuclear weapons has always been a major issue in international policy.

At the present time the only countries acknowledging to possess such weapons are the United States, Russia, the United Kingdom, France, China, India, Pakistan, and North Korea. It is widely believed that Israel possesses nuclear weapons, although it never acknowledged having them.

### **1.2.2 Types**

There are basically two types of nuclear weapons mentioned in open source information:

1. Devices that solely use nuclear fission for their destructive power.
2. Devices that use nuclear fusion to increase the total energy release.

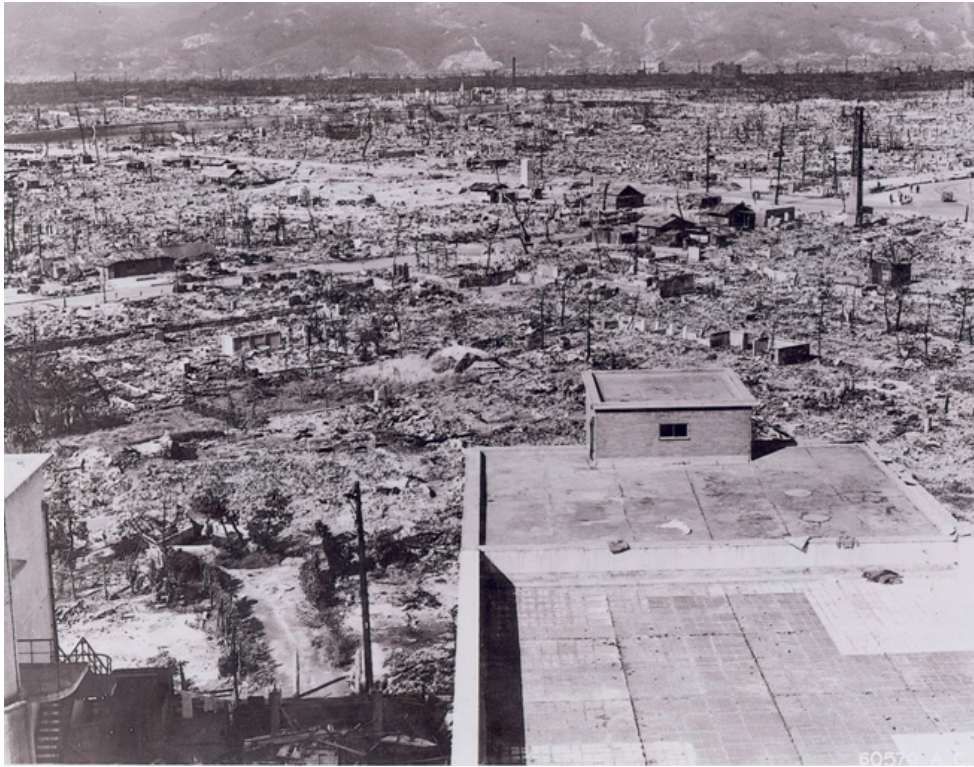


Figure 1.2: The city of Hiroshima after the nuclear explosion of the “Little Boy” device (13-18 kT). (Public domain)

The first type uses only nuclear fission. In such weapons conventional chemical explosives are used to rapidly bring fissile material into a supercritical mass. An assembly is called supercritical when the percentage of fission-produced neutrons captured by another fissile nucleus is large enough, so that each fission event induces more than one following fission events. Consequently, an uncontrolled nuclear chain reaction is started growing exponentially and releasing a great amount of energy within microseconds. The simplest method to accomplish this is used in the gun-type assembly by shooting one piece of subcritical mass into another. Typically, a projectile is shot onto a hollow set of rings both made of fissile material. However, once the two parts are close enough, the assembly becomes critical, meaning that every neutron set free by spontaneous fission may induce a nuclear chain reaction. If this happens too early

it causes the bomb to fizzle, blowing most of the still unused fuel apart (so called pre-detonation). Since weapons-grade plutonium ( $^{239}\text{Pu}$  with less than 7%  $^{240}\text{Pu}$ ) is always contaminated with  $^{240}\text{Pu}$ , which increases the neutron rate from spontaneous fission, a gun-type bomb is thought to only be practical with enriched uranium. This method was applied in the “Little Boy” bomb, that detonated over Hiroshima with an estimated yield of 13 – 18 kt TNT equivalent, which corresponds to somewhat more than 1 percent efficiency [Glasstone, 1977] [Bernstein, 2008].

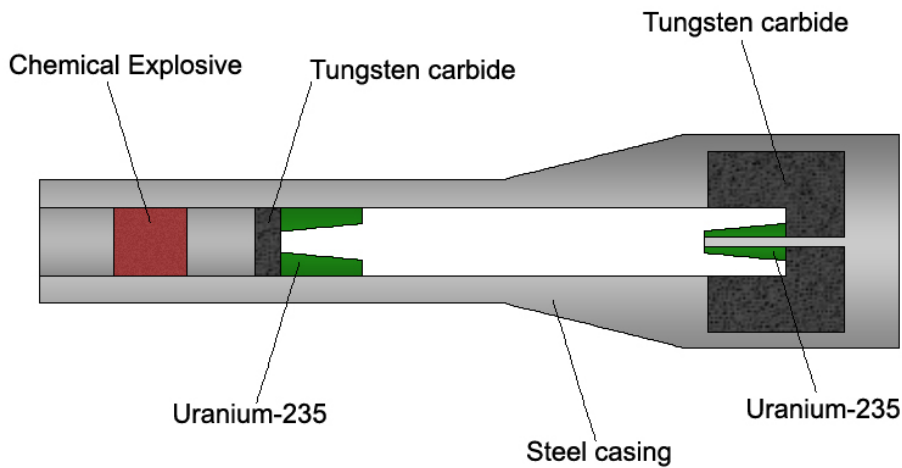


Figure 1.3: A schematic view of a gun-type fission bomb

A more sophisticated approach is the implosion assembly method, which derives the detonation energy from compressing a subcritical mass into a supercritical. It is possible to use weapon grade uranium as well as weapons-grade plutonium for this type, although plutonium is the standard material since the early 1960s. A quite inefficient design is the linear implosion type, where two

conventional explosives facing each other compress the ovoid formed plutonium fuel into a sphere. Explosives arranged in a spherical symmetrical way around the plutonium are most effective. It is aimed to keep the supercritical mass together as long as possible to ensure many fission reactions to happen. For this reason a tamper, especially dense and heavy material surrounding the plutonium, most commonly  $^{238}\text{U}$ , is used to pick up the impulse of the implosion and due to its inertia enabling a longer reaction time. It is a major challenge to create a homogeneous shock wave towards the center, so a subtle arrangement as well as precise timing of the explosives is crucial for its “successful” outcome. Like the first man-made nuclear explosion (“Trinity”; see next chapter) the “Fat Man” bomb that destroyed Nagasaki was an implosion type bomb. It had a yield of about 21 kt and an estimated 17 percent efficiency [Glasstone, 1977], [Bernstein, 2008].

The second type of nuclear weapon uses nuclear fusion either to improve the implosion design or to produce a large amount of its energy out of fusion. In so called fusion boosted fission bombs the energy provided by fusion is negligible. The high pressure of the implosion is used to start fusion reactions in a mixture of tritium and deuterium. The hydrogen isotopes fuse to helium also producing free neutrons, which are used to boost fission reactions in the plutonium pit. The amount of fissile material can be significantly reduced by this method, which reduces the size of the device while keeping the same destructive energy.

While pure fission or fusion-boosted fission weapons can be made to yield hundreds of kilotons equivalent to TNT, the most efficient way to build a nuclear weapon is realized in multi-stage thermonuclear weapons. The basic idea is to connect different parts of a weapon in “stages”, with the detonation of the first stage providing the energy to induce the second stage and so on. This principle is realized in the Teller-Ulam design, named after two of its main developers, Edward Teller and Stanislaw Ulam. They were the first to come up with the implosion by radiation principle, which was kept secret for nearly three decades and is colloquially referred to as the “H-bomb secret”. High levels of X-ray radiation are set free by the first stage, usually an implosion design fission bomb,



are reflected by the weapon's outer casing and used to compress the pusher of the secondary stage, which contains the fusion fuel. The energy of the radiation is captured by a highly absorbing material, such as styrofoam, creating a strong radial inward momentum. The pusher is usually made out of  $^{238}\text{U}$  and has the function of holding the fusion fuel together inertially. Additionally, because of its ability to undergo fission induced by high energy neutrons set free by the fusion reactions, the pusher also serves as a chief energy source.

The first two-stage thermonuclear bomb "Ivy Mike" detonated on 1 November 1952 on the Enewetak atoll in the Pacific and had a yield of around 12 Mt equivalent to TNT. The fusion fuel consisted out of a mixture of cryogenically cooled liquid tritium and deuterium, which was extremely sumptuous (the cooling system alone weighed around 18t). Since lithium was found to be a practical tritium producer ( $^7\text{Li}(\text{n}, \text{n}\alpha)^3\text{H}$  and  $^6\text{Li}(\text{n}, \alpha)^3\text{H}$ ) a mixture of lithium and deuterium was normally used as fusion fuel.

The secondary stage is usually shown as a column of fusion fuel surrounded by the pusher and including a "spark", a subcritical assembly of fissile material like  $^{239}\text{Pu}$ . Once the fusion fuel together with the spark is compressed and heated by the pusher, the spark becomes supercritical and fission reactions begin to release neutrons. The neutrons interact with lithium in the fusion fuel creating tritium. Because of the high temperature and pressure, fusion reactions are induced creating even more neutrons. In this high neutron flux the  $^{238}\text{U}$  of the pusher undergoes fission [Rhodes, 1995]. The Castle Bravo test, that was conducted by the United States in 1954, had, for example, a total yield of 15 Mt whereof around 10 Mt were derived of the  $^{238}\text{U}$  pusher.

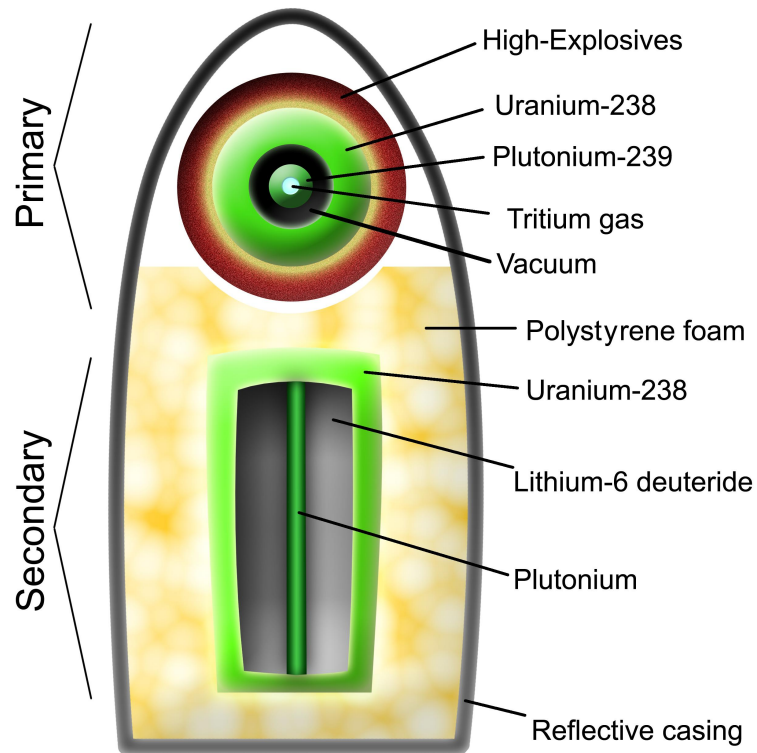


Figure 1.4: A possible realization of the Teller-Ulam design: The first stage is shown as a fusion-boostered implosion type bomb. The function of the reflective casing is to trap the radiation of the first stage inside and to direct it onto the secondary stage.

The tertiary stage, if one is present, would be placed below the secondary being very similar in design and made up of the same material as the secondary.

### 1.2.3 Nuclear weapons testing

The first detonation of a nuclear bomb was conducted on 16 June 1945 by the United States in the desert of New Mexico. “Trinity’s” purpose was to verify the implosion-type design as practicable since the scientists of the Manhattan

Project were very sure about the functioning of gun-type bombs like the “Little Boy”. With a total yield of between 20 kt and 22 kt, “Trinity” exceeded the developers predictions and the implosion-type design was then first deployed in the “Fat Man” bomb [Hoddeson et al., 1993].

After World War II the Soviet Union tested its first nuclear bomb “Joe 1” on 29 August 1949 marking the beginning of the nuclear arms race. Other countries followed: The United Kingdom carried out its first nuclear weapons test in 1952 followed by France in 1960, China in 1964, India in 1974, Pakistan in 1998 and North Korea in 2006.



Figure 1.5: The fireball of the “Trinity” test, 0.016 seconds after detonation, with a diameter of about 200m. In the foreground, trees are pictured as small black dots. Picture taken from [LANL, 2009].

On 1 November 1952 the first fusion bomb “Ivy Mike” was tested by the United States. Two years later the “Castle Bravo” test at the Bikini Atoll

created massive international concern when its fallout poisoned inhabitants of the atolls of Rongelap, Rongerik and Utrik as well as the crew of the Japanese fishing trawler “Lucky Dragon”. One member of the trawler crew died from radiation sickness and many of the islands inhabitants suffered from radiation burns and later from radiation related diseases as well as an increased rate of cancer and birth defects. This was probably the worst U.S. nuclear incident and it globally called attention to the hazards of nuclear testing. Nevertheless thermonuclear weapons were tested by many other countries such as the Soviet Union, the United Kingdom, France and China.

In 1961 the Soviet Union tested the “Tsar”, the largest and most powerful nuclear weapon ever detonated. It had a total yield of about 50 Mt and consisted out of three stages. To reduce the radioactive fallout, which would have probably hit Soviet territory, it was decided to replace the  $^{238}\text{U}$  pusher by lead. Otherwise the yield was estimated to be around 100 Mt. As a matter of fact, the Tsar was one of the “cleanest” bombs, since approximately 97% of the total yield was provided by fusion reactions [Khariton and Smirnov, 1993]. The most recent nuclear tests in history were performed by North Korea in 2006 and 2009. Altogether over 2000 nuclear tests were carried out all over the world since 1945.

Nuclear weapons tests are divided into categories according to the environment of the test [Glasstone, 1977]:

- Atmospheric testing refers to explosions in or above the atmosphere. Typically, these are realized by mounting a nuclear bomb on top of a tower, planting it on the ground, elevating it with a balloon or dropping it from an airplane. Close to the ground nuclear explosions generate a distinctive mushroom cloud of dirt and debris. Although any kind of explosion, powerful enough, can form such a mushroom cloud, it is inseparably associated with nuclear weapons. Atmospheric tests produce large amounts of radioactive fallout compared to underground or underwater tests.
- Underground testing is performed under the surface of the earth. This type of testing was applied in the majority of all nuclear tests that were carried out since 1963. Depending on the depth and the bomb yield, the

soil can provide a shielding from the atmosphere. The enormous heat of the explosion often leaves behind a sphere of glazed rocks and stones almost fully containing radioactive fallout. However, when the roof of the cavity collapses subsidence craters are formed and radioactive debris can be set free into the atmosphere. Usually an underground test results in seismic activity proportional to the yield of the nuclear device but also depending on the materials of the surrounding soil.

- Underwater testing covers test detonations carried out under water or close to the surface of water. In history there were comparatively few tests of this nature. Their typical purpose was to evaluate the effects of nuclear weapons against naval vessels. The depth beneath the water surface has a major influence on the effects of the explosion. Shallow underwater explosions are able to lift huge masses of water to heights of several thousands of meters in a column-like form. Deep underwater explosions, on the other hand, usually direct a large amount of the energy into forming surface waves and are therefore particularly able to devastate coastal areas. Both types create underwater shockwaves that can be recorded hydroacoustically. In addition to fission products, radioactive water and steam are dispersed into the atmosphere.

Beyond that, nuclear tests are often categorized by the purpose of the test itself. Weapon-related tests are conducted to investigate the functioning and behavior of the weapon design, whereas weapon-effect tests are to analyze the effects on organisms and structures. Nuclear testing has also been used for clearly political purposes. The Tsar bomb, that was mentioned earlier, is a perfect example for this since it was too large and heavy to be practically used against an enemy target. The Tu-95V plane needed to be modified in order to carry the 26 t of weight. Additionally, efforts have been made to use nuclear explosions peacefully for economic reasons. There were a variety of objectives from deep seismic sounding, creating underground storage cavities or reservoirs and helping to construct a canal. The United States and the Soviet Union both had Peaceful Nuclear Explosions (PNE) programs and conducted several nuclear tests to gain

information about its feasibility. However, no PNE project could justify the risks and the expenses involved and so the idea was eventually dropped.

## **1.3 The CTBT**

During the cold war the United States of America and the Soviet Union and their respective allies competed for supremacy in nuclear warfare. A great number of nuclear bomb tests have been conducted on both sides at this time. Together with the aim to slow down the arms race, concerns about radioactive fallout led to the mutual wish for a regulating treaty. On 5 August 1963 the Partial Nuclear Test Ban Treaty (PTBT), prohibiting all test detonations of nuclear weapons on ground surface, in the atmosphere, under water and in outer space, was opened for signature. Underground tests, however, were not banned by this treaty. The PTBT was signed by the USA, the Soviet Union and many other countries excluding, however, for example France and China. Five years later, on 1 July 1968, the first treaty to limit the spread of nuclear weapons, the Nuclear non-Proliferation Treaty (NPT), was agreed upon. Its main objectives are often referred to as the three pillars: 1. non-proliferation 2. disarmament 3. the right to use nuclear technology peacefully. The International Atomic Energy Agency (IAEA) is in charge of controlling the compliance with the treaty as its inspectorate. Each member state agrees to accept safeguards of the IAEA to verify that they are not diverting nuclear energy technology from peaceful uses to nuclear weapons or other nuclear explosive devices. At the moment only four countries with nuclear capabilities are not parties to or withdrew from the treaty: India, Israel, Pakistan and North Korea. With the end of the cold war the interest for a new more restrictive test ban treaty arose. On 24 September 1996 the Comprehensive Nuclear-Test-Ban Treaty (CTBT), banning all kind of nuclear test explosions, was opened for signature. The total ban of any type of nuclear weapon testing is to be seen as a major step in the process of nuclear disarmament [UNGA, 1996]. Furthermore without the opportunity to test new developments it constricts the qualitative improvement and the upcoming of

more advanced types of nuclear weapons.

Article 1 of this treaty expresses its main essence:

- 1. Each state party undertakes not to carry out any nuclear weapon test explosion or any other nuclear explosion, and to prohibit and prevent any such nuclear explosion at any place under its jurisdiction.*
- 2. Each state party undertakes, furthermore, to refrain from causing, encouraging, or in any way participating in the carrying out of any nuclear weapon test explosion or any other nuclear explosion.*

The CTBT will enter into force 180 days after all 44 so-called "Annex 2 states", which are the states that participated in the negotiations and had nuclear power plants or research reactors at that time, have signed and ratified the treaty. Until then the Provisional Technical Secretariat (PTS) for the CTBT Organization (CTBTO) is in charge of establishing a global alarm system and promoting the signing and ratification procedures. The PTS consists of three technical divisions: the International Monitoring System (IMS) division, the International Data Center (IDC) division and the On-Site Inspection (OSI) division [Hoffmann et al., 1999]. The IMS division has the task to create a reliable verification system, which is being built up at the moment. The IMS will consist of 170 seismic, 11 hydroacoustic, 60 infrasound and 80 radionuclide stations (80 particulate stations of which 40 will also have capabilities for noble gas measurements)[Dahlman et al., 2009]. In addition, there will be 16 certified radionuclide laboratories available for remeasuring samples in order to check the results from radionuclide particulate stations. All collected monitoring data is transmitted to the IDC, where it is processed, manually reviewed and analyzed. The results are presented to all member states as bulletins and reports [Matthews and De Geer, 2005]. On-site inspections represent the final verification measure: Every

member state has the right to call for an on-site inspection and present a request to the Executive Council, the executive organ of the CTBTO. It consists of 51 elected members from six different regions of the earth. For a decision to proceed, at least 30 members are required to vote in favor of an on-site inspection. During such an inspection, facts are gathered to leave no doubt whether a nuclear explosion took place or not. It is to be carried out by inspectors from member states supported by the Technical Secretariat [Dahlman et al., 2009].

While seismic, infrasound and hydro-acoustic monitoring can determine if an explosion took place, only radionuclide monitoring can verify the source as a nuclear explosion [De Geer, 1996]. Non-gaseous fission products are able to form particulates and mix with air as aerosol particles, which can be trapped by filters. In the past, several nuclear test explosions in the atmosphere were detected through particulate monitoring. However, it is rather unlikely for aerosols produced in an underground nuclear test to leave the soil in a detectable amount. Noble gases are chemically inert and are, therefore, most likely to be observed, even from an underground source. They can migrate to the surface along geological faults and cracks, especially when drawn by low barometric pressure.

In 1999 the International Noble Gas Experiment (INGE) was launched with the aim to develop noble gas systems suitable for IMS purposes [Auer et al., 2004]. The main criterion is that the Minimum Detectable Concentration (MDC) of  $^{133}\text{Xe}$  has to be 1 mBq/m<sup>3</sup> or lower for a 24 h period of sampling [Schulze et al., 2000]. The USA, Russia, France and Sweden each contributed by building different systems: ARSA, ARIX, SPALAX and SAUNA respectively. With exception of the SPALAX system, which uses high resolution gamma spectroscopy, all systems now use beta-gamma coincidence techniques. They were all tested in Freiburg in 2001 and were proven to fulfill the demands of the IMS network [Auer et al., 2004]. At the moment three systems are being deployed at monitoring stations around the world. In addition to that, mobile versions of the ARIX and the SAUNA systems that are able to perform on-site inspections have been developed.



## 1.4 Sources of radioxenon

### 1.4.1 General

Despite their rather short half-lives (see Table 1.1) radioxenon isotopes can be found in almost every region of the earth. The reason for the global radioxenon background is a continuous production in different nuclear facilities. Nearly all radioxenon in the atmosphere is of anthropogenic origin and its regional background concentration can vary from station to station depending how many and which radioxenon sources are close [Saey and De Geer, 2005].

Isotope	Half-life
$^{131m}\text{Xe}$	11.84 d
$^{133m}\text{Xe}$	2.19 d
$^{133}\text{Xe}$	5.24 d
$^{135}\text{Xe}$	9.10 h

Table 1.1: Radioxenon isotopes of interest and their half-lives

To facilitate the verification of compliance with the CTBT it is important to distinguish civil sources from nuclear explosions. The factors that are responsible for the difference in isotopic activity ratios relate on the small time window of about one microsecond in which most fissions during a nuclear explosion take place. Most fissions, therefore, are induced by fast unmoderated neutrons, which results in different fission yields (see figure 1.1). Additionally there is little time for activation products to build up. Contrary to that, in a nuclear reactor most fissions are induced by moderated neutrons and there is a lot of time for activation products to build up. These two effects lead to different isotopic signatures.

### 1.4.2 Civil sources

There are a number of possible civil sources of fission products including the four CTBT relevant xenon isotopes: nuclear power plants, nuclear research reactors, fuel reprocessing plants and radiopharmaceutical sources [Saey, 2007].

In October 2009, 436 nuclear power reactors providing over 370 GW of total power output were in operation worldwide [PRIS, 2009]. In nuclear power plants fissile material together with a moderator create a controlled nuclear chain reaction. Control rods containing neutron absorbing material are used to keep the rate of fissions at a safe level. The average total energy produced in one fission of  $^{235}\text{U}$  is 200 MeV. Most of the energy is carried by the fission products producing heat, which is converted into electrical power by a steam turbine. The fuel rods consist of the fuel itself and a cladding. Usually uranium oxide or uranium oxide mixed with plutonium oxide pressed to small pellets is used as fuel. Since zirconium has a very low neutron capture cross section, alloys with a high percentage of zirconium like Zircalloy ( $\sim 90\%$  zirconium) are the most common materials for the cladding. The purpose of the cladding is to seal the fuel from the coolant preventing fission products to leak out. However, corrosion, the exposure to high radiation and thermal stress, especially during start-up and shut-down, are well known problems that can cause cracks in the cladding. Also, traces of fissile material in the coolant itself or contamination on the surface of the cladding can set free radioxenon isotopes once they undergo fission. Additionally, fission products can leave the fuel rods during a reactor incident. The quantities released from a nuclear power plant depend very much on the containment of the facility and the circumstances, under which the release happens.

After a period of time a fuel rod comes to a point where it is no longer useful in sustaining a nuclear chain reaction and needs to be replaced with new ones. Nuclear reprocessing is often applied to fuel rods after they have cooled down for many months or some years in order to extract remaining fissile material and facilitate further waste management. For this purpose the cladding, still containing most of the fission products, is detached and the fuel is dissolved in

acid or a basic solution. The standard method for reprocessing nuclear fuel is PUREX (Plutonium and Uranium Recovery by Extraction). At the moment this is the most developed technique. For the extraction of plutonium and uranium a mixture of tributylphosphate and kerosene is used [Makhijani et al., 1995]. Most of the fission products set free during this process are removed by waste processing techniques, noble gases, however, are quite likely to escape. Most radioxenons will have decayed until then, although some might still be present from the spontaneous fission of  $^{240}\text{Pu}$ . So it is mainly  $^{85}\text{Kr}$ , a typical fission product as well, with a half-life of 10.8 a which is being released by fuel reprocessing plants [Winger et al., 2005].

In nuclear medicine radioactive isotopes are used for the diagnosis and treatment of diseases. The application of radiopharmaceuticals in molecular imaging has, in contrast to other imaging techniques (e.g. X-ray), the feature to depict metabolic processes. In therapeutic use, radiation sources external to the body (radiotherapy) and implanted radiation sources (brachytherapy) are often employed to treat diseases such as cancer or as palliative care. Most commonly used radioisotopes are  $^{99m}\text{Tc}$ ,  $^{133}\text{Xe}$  and  $^{201}\text{Tl}$  for imaging and  $^{90}\text{Y}$  as well as  $^{131}\text{I}$  for therapeutical purposes. The radioactive isotopes are produced within large hospitals and medical centers or in commercial radiopharmaceutical plants. There are basically two ways to produce a certain radioisotope of interest: by fission or via neutron activation, whereas the fission method is much more efficient. Both can be accomplished within a nuclear reactor. After a certain time of neutron irradiation the fission products and the neutron activation products are extracted chemically. The radioxenons built up from fission can escape into the atmosphere especially during chemical separation [Saey, 2009].

### 1.4.3 Releases from nuclear tests

A nuclear explosion takes place in a very short period of time. Within a microsecond the energy release from fissions becomes large enough to burst the critical assembly and end the chain reaction. Contrary to fission in a nuclear reactor, fission during a nuclear explosion is predominantly induced by fast unmoderated

neutrons, which results in slightly different yields. Additionally, because of the brief time span, neutron activation occurs to a minor extent.

A nuclear detonation with the power of one kiloton equivalent to TNT releases an amount of energy equal to  $4.2 \times 10^{12}$  J. In average, the total energy set free by the fission of one  $^{235}\text{U}$  atom is 200 MeV ( $3.2 \times 10^{-11}$  J) which splits up into following fragments:

- 165 MeV kinetic energy of fission products
- 7 MeV prompt  $\gamma$  radiation
- 6 MeV kinetic energy of neutrons
- 7 MeV excitation energy of fission products
- 6 MeV  $\gamma$  radiation from fission products
- 9 MeV antineutrinos from  $\beta^-$  decaying fission products

For one fission approximately 180 MeV are immediately available as energy, which makes about  $1.45 \times 10^{23}$  fissions per kiloton. According to the cumulative fission yield of the nuclear fuel inside the device the released activity can be calculated for each isotope. Looking at the three typical materials used in nuclear bombs ( $^{235}\text{U}$ ,  $^{238}\text{U}$  and  $^{239}\text{Pu}$ ), the cumulative fission yields of  $^{133}\text{Xe}$  lie between 4.86% for  $^{239}\text{Pu}$  and 6.02% for  $^{238}\text{U}$ , both induced by high energy neutrons (14.7 MeV) [England and Rider, 1994]. Thus, the number of  $^{133}\text{Xe}$  nuclei created lies between  $7.0 \times 10^{21}$  and  $8.7 \times 10^{21}$ . The activity can be calculated with:

$$A = \lambda \cdot N(t) = \frac{\ln(2)}{t_{1/2}} \cdot N(t)$$

and equals  $1.07 \times 10^{16}$  Bq respectively  $1.33 \times 10^{16}$  Bq [Saey, 2007]. Therefore, the initial release of a nuclear explosion with the power of 1 kiloton lies somewhere between these two values, according to the fuel composition. However, regarding the isobaric line of mass 133 nuclei, the activity concentration of  $^{133}\text{Xe}$  immediately after the nuclear chain reaction ends is quite low. Under the assumption

that the xenon isotopes are separated from their precursor isotopes at that time, possible in-growth is inhibited and the activity concentration measured is only depending on decay and the independent fission yields. Assuming full in-growth causes the full cumulative yields to be generated. Opposing to radioactive decay the rate of growth from precursors provokes the activity concentration to increase.

Type of facility	Order of magnitude of radioxenon release
Hospitals	$10^3$ Bq
Research laboratories	$10^6$ Bq
Nuclear power plants	$10^9$ Bq
Radiopharmaceutical plants	$10^{12} - 10^{13}$ Bq
1kton nuclear explosion underground	$10^{13} - 10^{15}$ Bq
1kton nuclear explosion atmospheric	$10^{16}$ Bq

Table 1.2: The estimated order of magnitudes of radioxenon release from different facilities and events. [Saey, 2007]

## 1.5 Environmental radioxenon background

To be able to distinguish civil radioxenon releases from nuclear explosions, the radioxenon background of ambient ground level air needs to be studied. As mentioned earlier, the first atmospheric radioxenon measurements were performed during World War II [Ziegler and Jacobson, 1995]. Later, in the 1960s, atmospheric samples were taken and measured by a group of scientists at the University of Heidelberg in order to find traces of  $^{85}\text{Kr}$  and  $^{133}\text{Xe}$  originating from nuclear weapon tests. In 1961 signals indicating a nuclear explosion have indeed been observed. Soviet nuclear weapon tests, conducted in the autumn of 1961, are believed to be the source [Ehhalt et al., 1963]. Since the 1970s the Integrated Monitoring and Information System (IMIS) of Germany is

recording radioxenon levels at seven different sites with a time resolution of one week [Stockburger et al., 1977]. Contrary to INGE systems, the total activity is measured by proportional counters integrating over all radioxenon isotopes. However, a separation of two isotopes can be done by decay analysis.

The longest series of uninterrupted  $^{133}\text{Xe}$  activity concentration data were recorded at the Freiburg station recorded from 1977 until 2009. The measured values lie between 1 mBq/m<sup>3</sup> and 100 mBq/m<sup>3</sup> with one maximum at 106 Bq/m<sup>3</sup>. It was the one day sample taken on 1 May 1986, a few days after the accident of Chernobyl.

The data from INGE systems within the IMS network contribute to getting a better understanding of the environmental radioxenon background. The data collected from six different stations in Europe between 2003 and 2008 are studied in [Saey et al., 2010b]: Longyearbyen (Spitsbergen, Norway), Stockholm (Sweden), Dubna (Russia), Schauinsland Mountain (Germany), Bruyères-le-Châtel and Marseille (France). Xenon-133 is the isotope most commonly seen in atmospheric samples. Nuclear power reactors and radiopharmaceutical plants are to be seen as the major sources. Thus it is regularly found at locations downwind from nuclear power plants. In regions with a high density of nuclear reactors, such as Central Europe, the mean activity concentration of  $^{133}\text{Xe}$  is found to be between 5 mBq/m<sup>3</sup> and 20 mBq/m<sup>3</sup>. At stations on the edge of that region, like the Stockholm station, the activity concentrations range from 1.4 mBq/m<sup>3</sup> to 2.4 mBq/m<sup>3</sup>. In the very remote area of Spitsbergen, far from nuclear reactors, a mean activity concentration accounts for 0.2 mBq/m<sup>3</sup>. In general, the radioxenon background in Europe does not show any seasonal changes, except the station at Spitspergen. In this case, atmospheric transport over long distances is believed to affect the distribution of radioxenon in the atmosphere and add a seasonal variability.

Today the average activity concentration of  $^{133}\text{Xe}$  in Germany lies around 6 mBq/m<sup>3</sup>. In 2006 a comprehensive field test was carried out in Seibersdorf, Austria. Within this campaign, mobile versions of the SAUNA and ARIX systems collected 16 atmospheric and five sub-surface gas samples. The activity concen-

tration of  $^{133}\text{Xe}$  was determined to be between  $0.3 \text{ mBq/m}^3$  and  $2.4 \text{ mBq/m}^3$  for most atmospheric samples. One pair of measurements, however, showed a rather high activity concentration:  $(17 \pm 1) \text{ mBq/m}^3$  were detected by the SAUNA system and  $(51 \pm 3) \text{ mBq/m}^3$  by the ARIX system [Axelsson, 2007].

## 2 Scope of work

The Comprehensive Nuclear-Test-Ban Treaty (CTBT) and its verification system represent the conceptional background for this work. In order to establish a reliable verification system different sources of radioxenon isotopes are modeled and experimentally examined. This can provide valuable information about the effects on the global radioxenon background. However, to this date experimental studies of radioxenon releases of nuclear research reactors are not found in literature.

Therefore two measurement campaigns, one in May 2009 and one in October 2009, have been conducted at the Atominstitut of Vienna (ATI) using the mobile SAUNA (Swedish Automatic Unit for Noble gas Acquisition) system, which was assembled at the reactor platform. These campaigns were sponsored by the CTBTO and the FOI in cooperation with the ATI of the TU Vienna.

The key objective of the experiments is to determine if there are releases of radioxenons at concentrations capable of measurement for the SAUNA system ( $> 1 \text{ mBq/m}^3$ ). Furthermore, it aims to determine the radioxenon signature of the reactor, i.e. the ratios of the different radioxenon isotopes. In addition to this the releases of the irradiation tubes, which contain normal air, are analyzed for the presence of radioxenon isotopes. A separate study focuses on the radioxenon production of highly enriched uranium targets (93%  $^{235}\text{U}$ ) while being irradiated inside an irradiation tube.

Estimations concerning possible sources, the transport and the intensity of the radioxenon release are performed and compared to the experimental results.



## 3 Theory

### 3.1 Characteristics of the four xenon isotopes of interest

#### 3.1.1 General

Xenon ( $_{54}\text{Xe}$ ) is a colorless and odorless noble gas. Like all noble gases it is in practice chemically inert. As a trace gas it is present in the Earth's atmosphere with 0.087 ppm by volume [CRC, 1987]. There are 38 known isotopes, seven of which are stable and two have half-lives over  $10^{14}$  years [ENSDF, 2009]. Additionally, there are six metastable states of xenon. Only eight isotopes respectively isomers have half-lives over six hours, which is the minimum required for CTBT purposes. From a nuclear weapon test only four of these are produced in sufficient amount as fission or activation products:  $^{131m}\text{Xe}$ ,  $^{133m}\text{Xe}$ ,  $^{133}\text{Xe}$  and  $^{135}\text{Xe}$ . These are the CTBT relevant xenon isotopes/isomers [De Geer, 2001]. The others ( $^{122}\text{Xe}$ ,  $^{125}\text{Xe}$ ,  $^{127}\text{Xe}$ ,  $^{129m}\text{Xe}$ ) are neutron deficient and therefore unlikely to be produced in fission or in a high neutron flux. Nevertheless some of them are produced in nuclear medicine: For example, to gain  $^{125}\text{I}$ , natural xenon is irradiated so that after the reaction  $^{124}\text{Xe}(n,\gamma)^{125}\text{Xe}$  the product decays to  $^{125}\text{I}$ . The possibility of sampling xenon from such a source certainly demands attention.

All CTBT relevant isotopes emit photons and beta or conversion electrons in coincidence. The SAUNA noble gas measuring system, which is described in detail later, uses beta-gamma coincidence techniques to create a two dimensional spectrum. In this chapter all nuclear data is retrieved from [ENSDF, 2009], if

not stated otherwise.

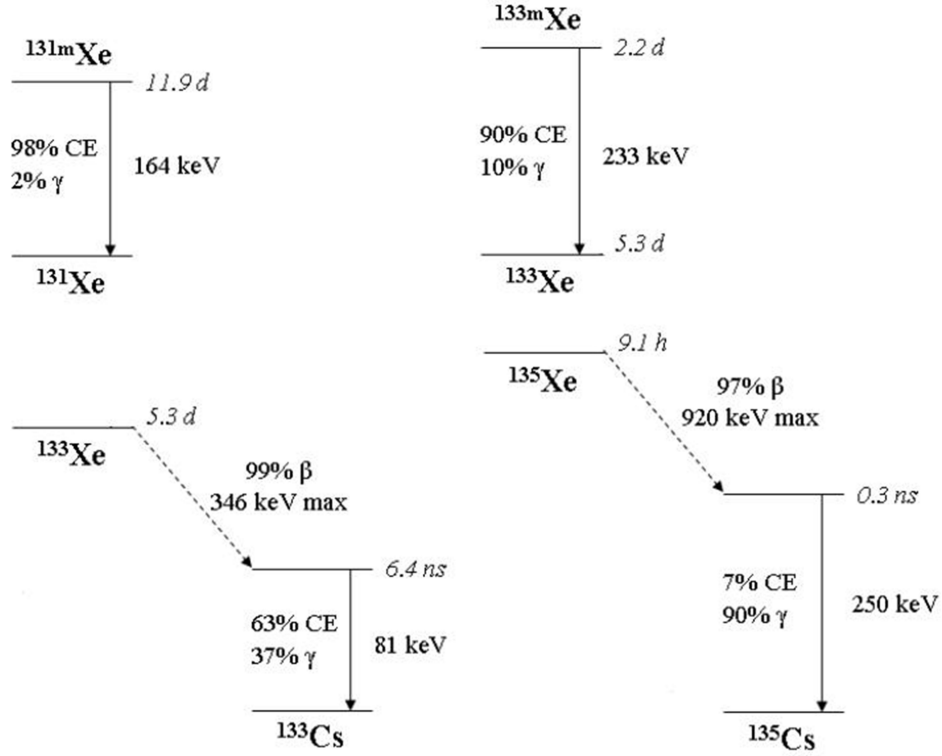


Figure 3.1: Decay schemes for  $^{131m}\text{Xe}$ ,  $^{133m}\text{Xe}$ ,  $^{133}\text{Xe}$  and  $^{135}\text{Xe}$

### 3.1.2 $^{131m}\text{Xe}$

Xe-131m is a fission product that is produced when nuclear fuel is irradiated. It is predominantly created by decay of  $^{131}\text{I}$ . Possible sources are reprocessing plants and nuclear reactors. Also, when  $^{133}\text{Xe}$  is gained for medical purposes  $^{131m}\text{Xe}$  will be present as a byproduct.

The heavily suppressed 163.9 keV ( $I = 1.95\%$ ) gamma transition is not coincident with any beta signal so it cannot be seen in a beta-gamma coincidence spectrum (but well in high resolution gamma spectrometry). Xe-131m primarily

decays by sending out conversion electrons. The K shell conversion electron at 129.4 keV ( $I = 61.6\%$ ) and the L conversion electron at 158.8 keV ( $I = 28.8\%$ ) are the most dominant ones. The conversion electrons are coincident with characteristic X-rays:  $K_\alpha$  around 29.7 keV and  $K_\beta$  around 33.5 keV. The L X-rays are all below 6 keV, where detector efficiencies are low, which makes them unfavorable. So  $^{131m}\text{Xe}$  is analyzed by its K conversion electron and the combined K X-rays ( $I = 54\%$ ).

### 3.1.3 $^{133m}\text{Xe}$

Xe-133m is produced as a fission product as well as through excitation of  $^{133}\text{Xe}$ . The main sources of  $^{133m}\text{Xe}$  are nuclear explosions and radiopharmaceutical facilities [Saey, 2007], [Saey, 2009].

With the half-life of 2.19 d it decays by isomeric transition to  $^{133}\text{Xe}$ . Again the gamma line at 233.2 keV ( $I = 8.2\%$ ) is not useful for analysis in beta-gamma coincidence spectrometry, since it is not coincident with any beta signal. Instead of that its K conversion electron at 198.7 keV ( $I = 63.2\%$ ) is in coincidence with X-rays,  $K_\alpha$  around 29.7 keV and  $K_\beta$  around 33.8 keV. Same as with  $^{131m}\text{Xe}$  the L conversion electrons are not practical.

### 3.1.4 $^{133}\text{Xe}$

Xe-133 is a main fission product. In nuclear medicine it is being used for lung function diagnostics. It is produced mainly by fission of  $^{235}\text{U}$  but also in smaller amounts by irradiation of natural xenon gas:  $^{132}\text{Xe}(n,\gamma)^{133}\text{Xe}$ . Xe-133 has a long history in the records of radioxenon monitoring: The first environmental measurements date back to World War II, when U.S. airplanes were used to sample air over Germany to find traces of a German nuclear program by analyzing it for  $^{133}\text{Xe}$  [Ziegler and Jacobson, 1995]. Decades later  $^{133}\text{Xe}$  was being measured during weapons tests. At that time  $^{133}\text{Xe}$  was only detected after an atmospheric or poorly contained underground test.

Xe-133 is a beta emitter: In 99.2% it decays to the first excited state of stable

$^{133}\text{Cs}$  with an end-point energy of 346 keV. The excited state has a 6.2 ns half-life decaying to the ground state via 81.0 keV photons ( $I = 38.0\%$ ) or via 45 keV conversion electrons ( $I = 55.1\%$ ) in coincidence with X-rays. The combined  $K_\alpha$  X-rays lie at 30.8 keV ( $I = 40.3\%$ ),  $K_\beta$  at 35.1 keV ( $I = 9.4\%$ ). Due to the short half-life of 6.2 ns, the conversion electron together with the X-rays can be seen coincident with the initial beta electron. This has the effect of adding 45 keV to the beta energy resulting in an end-point energy of 391 keV.

### 3.1.5 $^{135}\text{Xe}$

Of all discussed xenon isotopes  $^{135}\text{Xe}$  has the highest independent fission yield with  $7.8 \times 10^{-2}\%$ . This together with its high neutron absorption cross section of  $2.65 \times 10^6$  b at 0.025 eV make  $^{135}\text{Xe}$  an important reactor poison [KAERI, 2010]. Because it subducts neutrons from the reactor core it decreases the reactivity of a reactor. Reactor poisoning can even stop the nuclear chain reaction, when strong enough. It can represent a serious hazard in reactor operation, if it is dealt with incorrectly. Xe-135 is produced in large amounts in nuclear explosions. It is as well released from nuclear reactors, especially after reactor shut-downs, and from radiopharmaceutical plants.

Xe-135 decays via beta decay into  $^{135}\text{Cs}$ , mainly ( $I = 96\%$ ) into its first excited state ( $T_{1/2} = 0.28$  ns) at 294.8 keV. Again, because of the short half-life it is detected in coincidence with beta electrons (end-point energy: 901 keV). This coincidence is used for the quantification of  $^{135}\text{Xe}$ . Additionally there is a K conversion electron of 213.8 keV ( $I = 5.7\%$ ), which, together with coincident X-rays ( $I = 5.2\%$ ), has to be considered in analysis.

## 3.2 The SAUNA noble gas measuring system

### 3.2.1 General

The SAUNA system is an automatic xenon sampling and analyzing device. Together with the net count calculation method for data analysis it has been devel-

oped by the Swedish Defence Research Agency (FOI) [Ringbom et al., 2003]. It was designed and developed to be part of the monitoring network of the CTBTO. Within the IMS network the stationary SAUNA system is operated at 11 different locations worldwide. SAUNA consists of three main parts: a sampling, a processing and a detector unit. For the purpose of on-site inspections a mobile version, the SAUNA OSI system, has been developed. The mobile system only consists of the sampling and processing units. It collects xenon and stores it in exchangeable transport columns, which can be analyzed later by a detector unit or in a lab system.

At a flow rate of around  $1 \text{ m}^3/\text{h}$ , a four-hour-sample contains about  $0.3 \text{ cm}^3$  of xenon. For the most part this will be natural xenon and perhaps traces of radioxenon. In addition to that, the sample will contain about 80% helium, which is used as a carrier gas, but does not affect the later measurement at all. Radon, a naturally occurring noble gas, is tried to be separated out during sampling and processing. Especially  $^{222}\text{Rn}$ , which -of radon isotopes- has the longest half-life of 3.8 d, can survive sampling and processing and worsen the xenon sensitivity via its short-lived daughter nuclides. Nevertheless, traces of radon will be found in almost every sample.

### **3.2.2 The mobile SAUNA OSI field sampler**

The SAUNA OSI system is specifically designed for field use. Thus a main aspect in the development was to keep the system as simple as possible without being prone to environmental influences. It consists of eight portable boxes of about 20 kg each that can be set up and connected within a few minutes.

By cooling and filtering, the air is purged of aerosols, water and carbon dioxide. Of the remaining air xenon is extracted using adsorption on activated charcoal. Although the adsorption coefficient rapidly increases with decreasing temperature [Underhill, 1996], sampling is performed at room-temperature. SAUNA uses high pressure and long charcoal beds together with efficient concentration techniques to achieve adsorption. Hence it does not need liquid nitrogen or compressors to cool the charcoal, which has a positive effect on the systems

simplicity, size, power consumption and cost. To allow uninterrupted sampling, two sub-units, identical in construction, each able to collect xenon for up to 6 h. While one is sampling the other one undergoes desorption and regeneration.

A sampling pump sucks air and compresses it to an overpressure of about 8 bar. After this the air is being cooled down to  $-5^{\circ}\text{C}$  by a heat exchanger and thermoelectric coolers. This initially removes some of the moisture. A  $4\text{ \AA}$  molecular sieve then removes remaining water and carbon dioxide. After this, the air flows through four consecutive columns filled with coconut shell charcoal, where xenon is adsorbed. The pressure drop across the sampling unit is around 2 bar. Before the air reaches the air outlet a volume meter determines the volume of the sampled air.

The xenon collected during sampling can now be stored in a portable transport column to be analyzed later. An evacuation pump provides an underpressure of about 200 mbar when the sampling columns begin heating to about  $300^{\circ}\text{C}$ . Helium as a carrier gas is pulsed through the charcoal traps. This way xenon is transferred to charcoal traps within the transport column. Again, residual water and carbon dioxide are filtered in preceding  $4\text{ \AA}$  molecular sieves. Two molecular sieve columns together with one long spiral filled with activated charcoal make up one transport column. Once the transfer has finished, the transport columns can be disconnected and sent to a lab system. A more detailed description of the stationary system can be found in [Ringbom et al., 2003], however some details, like the system pressure, have changed by now [Lindh, 2009].

### 3.2.3 The SAUNA lab system

The lab system effectively comprises two parts: a gas chromatograph and the beta and gamma detectors. The gas chromatograph has two purposes: a further separation of xenon from other gases and the quantification of the total amount of extracted xenon.

Once the transport column is connected, it is being heated slowly while helium is pumped through. Because of the slow heating, light gases first begin to desorb from the activated charcoal. A thermal conductivity detector within the gas



Figure 3.2: A photograph of two transport columns.

chromatograph senses changes in the thermal conductivity of the flowing gas mixture. Since most gases have a thermal conductivity much less than that of helium, the resulting chromatogram shows directly the presence of gases other than helium. This way, xenon can effectively be separated from lighter gases and radon. The xenon peak appears about 30 minutes before the radon peak. To determine the total volume of the xenon peak, the thermal conductivity detector needs to be calibrated. This is done before all measurements by injecting a known volume of stable xenon into the gas chromatograph carried by a helium flow. During the time window of the xenon peak, the gas flow is directed to the detector unit. The total output volume, however, is about  $50 \text{ cm}^3$  whereas the detector cell volume is only  $6.4 \text{ cm}^3$ . A volume reduction is achieved by an aluminum column with 12 cm length and 3 mm in diameter including 0.5 g of carbogenic molecular sieve (CMS). Xenon is able to adsorb to the CMS before the residual carrier gas is evacuated. Then the column is heated to  $350^\circ\text{C}$  and the sample is transferred into the detector cell, that has already been evacuated. This is performed by a combination of volumetric transfer and carrier gas. The sample volume in the detector cell accords to  $6 \text{ cm}^3$ . This means that, assuming

1 cm<sup>3</sup> xenon in one typical sample, it still contains about 5 cm<sup>3</sup> of carrier gas and traces of other gases.

The activity of the sample is measured by beta-gamma detectors. A cylindrical plastic scintillator works as a beta detector. It is produced by Bicron from BC404 material. The sample is injected into the volume inside the scintillator cell with a small stainless steel pipe. The plastic scintillator resides in a hole in the middle of a NaI(Tl) crystal, which is used as a gamma detector. Photo multipliers (PMs) are arranged on both ends of the scintillator cell as well as on the NaI(Tl) crystal and are connected to the electronic readout set-up.

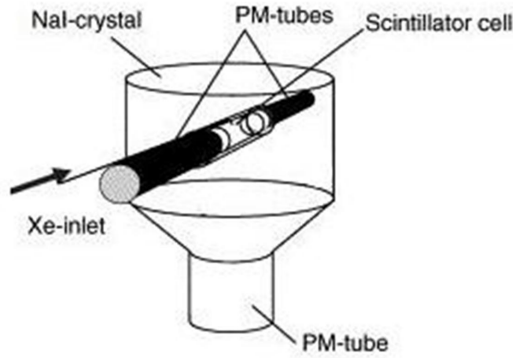


Figure 3.3: Schematic view of the detector system. Picture taken from [Ringbom et al., 2003]

### 3.2.4 Detector calibration

The detectors need to be calibrated in energy and efficiency. Different techniques are applied for the calibration of the detector system [Reeder et al., 2004], [Saey and De Geer, 2007]:

- Gamma energy calibration

The NaI(Tl) detector is calibrated in a standard way by using point sources while the beta-coincidence requirement is bypassed. Providing several use-



ful peaks in the energy range of interest, the most commonly used nuclides are:  $^{152}\text{Eu}$  with useful gamma peaks at 121.8, 163.9, 244.7 and 344.3 keV and  $^{137}\text{Cs}$  which has one gamma line at 661.7 keV.

- Beta energy calibration

The beta energy calibration of the plastic scintillator cell is performed utilizing Compton scattering from a gamma source external to the detector [Reeder et al., 2004]. The 661.7 keV photons of  $^{137}\text{Cs}$  are used for this, while the detector system is recording in beta-gamma coincidence mode. Incident gammas scatter in the scintillator material, producing a free recoil electron. The recoil electron is likely to be stopped within the plastic scintillator, giving off its total kinetic energy. The scattered gamma is measured in the NaI(Tl) detector. Of course, not every Compton scattering event in the plastic scintillator will deliver a useful signal: The recoil electron could leave the plastic scintillator or the scattered gamma could leave the NaI(Tl) crystal without being detected. But in general, the 2D array will show a distribution of events along a diagonal line on which the added energies of the beta and gamma detectors equal the full energy of the incident gamma. Now, if a single gamma channel is selected, the corresponding beta spectrum will show a peak. The energy of this peak is given by the Compton equation:

$$E_{\beta} = E_0 - E_{\gamma} \quad (3.1)$$

$E_{\beta}$  ... the beta energy

$E_0$  ... the energy of the initial gamma (661.7 keV)

$E_{\gamma}$  ... the energy of the scattered gamma

The beta calibration curve can now be obtained by correlating the beta energy ( $E_{\beta}$ ) given through equation 3.1 to the channel number of center of the Gaussian fitted peak. However, this does not take into account the resolution broadening of the beta and gamma detector. This causes small energy shifts, which can be evaluated by Monte Carlo N-Particle modeling.

The total energy shift is given as [Reeder et al., 2004]:

$$\Delta E = 25.33 \text{ keV} - 0.1215(E_\beta) + 0.0001646(\text{keV})^{-1}(E_\beta)^2 \quad (3.2)$$

$\Delta E$  ... energy shift

$E_\beta$  ... the uncorrected beta energy [keV]

- Efficiency calibration

The total beta-gamma efficiency  $\epsilon_{\beta\gamma}$  can be obtained after the gamma efficiency  $\epsilon_\gamma$  and the beta efficiency  $\epsilon_\beta$  were determined using following simple relation:

$$\epsilon_{\beta\gamma} = \epsilon_\beta \times \epsilon_\gamma \quad (3.3)$$

In a series of measurements, samples of the isotopes  $^{133}\text{Xe}$ ,  $^{222}\text{Rn}$  and  $^{131m}\text{Xe}$  are filled into the detector. The isotopes  $^{133}\text{Xe}$  and  $^{222}\text{Rn}$  are used to obtain the relative photon efficiency for the entire relevant energy range, while the absolute efficiency is determined measuring a  $^{131m}\text{Xe}$  sample. In case of  $^{133}\text{Xe}$ , which shows peaks at 32 keV and 81 keV, the relative efficiencies are related to each other:

$$\epsilon_\gamma(81) = \frac{I_{81}}{I_{32}} \times \frac{R_{32}}{R_{81}} \times \epsilon_\gamma(32) \quad (3.4)$$

$I_{81}$  ... measured intensity of the peak at 81keV

$I_{32}$  ... measured intensity of the peak at 32keV

$R_{81}$  ... branching ratio for the 81keV gamma decay

$R_{32}$  ... branching ratio for electron conversion

The same applies for  $^{214}\text{Pb}$ , a daughter nuclide of  $^{222}\text{Rn}$ , which has gamma lines at 242 keV, 295 keV and 352 keV. In addition to that it has several unresolved X-rays between 75 keV and 87 keV. Assuming that the relative efficiency does not change drastically, the X-ray region around 80 keV is assigned to the efficiency  $\epsilon_\gamma(81)$  at 81 keV. By doing this, the relative efficiency curve for the gamma region between 32 keV and 352 keV can be found.

Now the total efficiency can be calculated. Two spectra of a  $^{131m}\text{Xe}$  sample are recorded: one in beta singles and one in beta-gamma coincidence mode. The comparison of the 129 keV conversion electron peak area in the beta spectrum with the same peak in the beta-gamma spectrum gives a measure of the total efficiency, because the conversion electron is coincident with a 32 keV photon:

$$\epsilon_{\gamma}(32) = \frac{I_{xray}}{I_{tot}} \quad (3.5)$$

$I_{xray}$  ... measured intensity of the peak in coincidence with X-rays

$I_{tot}$  ... measured total intensity of the beta peak

With the relative efficiencies and the absolute efficiency at 32 keV at hand, the absolute gamma efficiencies can easily be calculated for the entire energy region.

The total beta efficiency is acquired by comparing the total intensity of the photon peaks of e.g.  $^{133}\text{Xe}$  (32 keV and 81 keV) obtained in gamma singles mode to the same peaks in a beta-coincident 2D spectrum. Integrating the beta distribution at a certain gamma energy gives the electron-coincident intensity for one ROI, divided by the total intensity that gives the total efficiency:

$$\epsilon_{\beta}(integrated) = \frac{I_{co}}{I_{tot}} \quad (3.6)$$

$I_{co}$  ... measured intensity of the  $\gamma$ -peak coincident with beta particles

$I_{tot}$  ... measured total intensity of the gamma peak

With the knowledge of  $\epsilon_{\beta}$  and  $\epsilon_{\gamma}$  the beta-gamma efficiency is given via equation 3.3.

## 3.3 The TRIGA Mark II reactor

### 3.3.1 Design and physical properties

TRIGA reactors are open-pool reactors used for TrainRing, Research and Isotope production and are produced by General Atomics. They are widely spread over the world and reach from 10 kW to 14 MW (thermal) in continuous power output. It is an inherently safe design, meaning that safety is guaranteed by the laws of nuclear physics, rather than engineering.

On March 7 1962 the TRIGA Mark II reactor of the Atominstitut of Vienna went critical for the first time. The reactor has a maximum continuous power output of 250 kW. As of the time of both experimental campaigns, the core contained 84 circular arranged fuel rods. A start-up neutron source (Sb-Be) is placed on the outmost edge of the reactor core. As long as all of the three control rods, which use boron carbide as absorber material, stay inserted, the assembly remains subcritical. Withdrawing the control rods from the core lets the reactor become critical and after roughly one minute the maximum power output is reached. The fuel rods contain a mixture of enriched uranium and zirconium-hydride. Zirconium-hydride works as the main moderator. Most of the neutrons, generated by fission, are moderated by the hydrogen nuclides inside the fuel. Zirconium-hydride has a negative temperature coefficient, which means with increasing temperature the efficiency as a moderator decreases. Unmoderated neutrons, however, are more unlikely to induce fission reactions, due to the  $1/v$  dependence of the fission cross section. This is sometimes referred to as the warm neutron principle and it is the reason for the inherent safety of the reactor. Three different types of fuel rods are being used:

Fuel material	Type 102	Type 104	Type 110(FLIP)
Uranium content	8.5wt.%	8.5wt.%	8.5wt.%
Enrichment	20% <sup>235</sup> U	20% <sup>235</sup> U	70% <sup>235</sup> U
H/Zr ratio	1.0	1.65	1.65
Cladding			
Material	aluminum	stainless steel	stainless steel
Wall thickness	0.76 mm	0.51 mm	0.51 mm
Dimensions			
Outer diameter	37.5 mm	37.5 mm	37.5 mm
Length	72.06 cm	72.06 cm	72.06 cm

Table 3.1: The three different types of fuel rods

The reactor can also be operated in a pulsed mode: During the time span of 40ms the maximum neutron flux increases from  $1 \times 10^{13} \text{ cm}^{-2}\text{s}^{-1}$  to  $1 \times 10^{16} \text{ cm}^{-2}\text{s}^{-1}$  and the thermal power output from 250 kW to 250 MW. The temperature inside the core rises to 360 °C during a pulse, compared to 200 °C during normal operation at 250 kW. Because of the negative temperature coefficient the increasing temperature reduces the reactivity and brings the power level back into the kW-range. The reactor is equipped with six dry irradiation tubes, that lead from the pool surface down to the reactor core, one of which right into the middle of the core.

On December 12 1984 during a practical training course a fuel element failure occurred while the reactor was operated in pulsed mode [Böck et al., 1987]. During the next days, an increased activity was observed in the reactor hall. The aerosol detector registered up to 800 counts per second, which is a considerable increase to the usual value of about 20 to 30 counts per second. The measured activity then decreased by time and converged the normal value. A second reactor pulse again led to an increased activity measured in the reactor hall, so it was clear that a damage of the fuel rod cladding had occurred.

Damages to the cladding of fuel elements can originate either from mechanical stress or chemical reactions. Cladding corrosion can be prevented by the use of high-purity water, a conductivity of less than  $0.1 \mu\text{S}/\text{cm}$  is desirable. Mechanical damage can arise out of thermal stress or when fuel rods are frequently handled, as in a research reactor.

### 3.3.2 Fuel inventory and estimated radioxenon emissions

The burn-up of the fuel is very small due to the low power level of the reactor. Many of the fuel elements that were loaded into the core in 1962 are still in operation. Burn-up calculations were performed for every single fuel element using the reactor physics software ORIGEN 2.2 [Khan, 2010]. In support of these calculations, a number of fuel elements were analyzed for  $^{137}\text{Cs}$  concentrations showing good agreement with the calculations. As a byproduct the amount of  $^{235}\text{U}$  was obtained for every fuel element. According to this the total amount of  $^{235}\text{U}$  within the core was calculated to be 3561 grams on June 30, 2009.

In [Fouquet et al., 2003] it is reported that the cladding provides total clad integrity at temperatures up to  $1150^\circ\text{C}$ . Furthermore, the UZrH fuel itself should retain 99.9% of all volatile fission products even without any cladding. The  $^{133}\text{Xe}$  equilibrium inventory of a reactor constantly operated at 250 kW yields a total  $^{133}\text{Xe}$  activity of  $5.8 \times 10^{14} \text{ Bq}$  [De Geer, 2009]: A damaged cladding of one of the 84 elements assumed, 0.1% could leak through giving a total activity of around 7 GBq. Estimating a tent volume of about  $10 \text{ m}^3$  and 100% effective transport would yield  $0.7 \text{ GBq}/\text{m}^3$ . Such an activity would cause a huge signal for the SAUNA. However, an unnoticed leak is not very probable.

Conditional to manufacturing fuel elements are often slightly contaminated on the outside. A typical value commonly used at CERCA-AREVA is a maximum alpha contamination of  $1.7 \text{ Bq}/\text{dm}^2$  [Böck, 2009]. The surface of a single fuel element lies around  $0.085 \text{ m}^2$ . For 84 fuel elements this gives a maximum total alpha contamination of 1214 Bq. Further, assuming an overall concentration of 20%  $^{235}\text{U}$  and 80%  $^{238}\text{U}$  leads to a total amount of  $9.3 \times 10^{-3} \text{ g}$  of  $^{235}\text{U}$  outside the fuel elements. This equals to around 0.02% of an average fuel elements

inventory of  $^{235}\text{U}$  resulting in an  $^{133}\text{Xe}$  activity concentration of approximately  $0.1 \text{ GBq/m}^3$  in the plastic tent. Note that this approximation is not considering the burn-up for the time the fuel rod spent in the reactor core, nor the dissolution of uranium into the reactor water and its constant removal by an ion exchanger, which cleans the reactor water. Taking this into account will probably lead to a much smaller total amount of  $^{235}\text{U}$  outside the fuel elements.

### 3.3.3 Transport of xenon through the reactor

Neglecting the contamination outside the fuel elements, radioxenon isotopes are mainly produced within the fuel meat. Subsequently, for radioxenon to be measured above the pool surface it has to overcome the barrier of the cladding, migrate through the pool water and into the air.

Assuming a leak in the cladding, through which xenon could be released into the water, three different processes are possible [De Geer, 2009]:

1. Diffusion followed by emanation:

The diffusion constant of xenon in water is  $(D = 2.2 \pm 0.4) \times 10^{-5} \text{ cm}^2/\text{s}$  [Wolber et al., 1998]. The diffusion length ( $L_D = 2\sqrt{Dt}$ ) is the characteristic scale measuring how far the substance has propagated through the medium in the time  $t$ . For the time span of one day, this gives a diffusion length of 2.7 cm. Thus, classical diffusion as means of transport can be neglected.

2. Convection followed by emanation:

Convection is naturally established during reactor operation due to temperature differences in the reactor water. Arguably, convection can provide mixing much quicker than through diffusion. Assuming total mixing of xenon in the water, there would still be the problem of emanation from the water surface into the air. This, however, would probably be a rather slow process.

3. Gas bubbles bursting at the water surface:

During continuous operation the fuel elements can heat up to 200 °C. This causes gas bubbles to constantly form at the surface of the fuel elements and rise to the pool surface once the buoyancy overcomes the contact forces. This process is frequently observed at the TRIGA reactor in Vienna. It seems reasonable that leaking radioxenon can get caught and transported to the surface within the steam bubbles.

On the whole it is safe to say, that the role of classical diffusion in the transport of xenon through the reactor water is negligible. The most probable way for radioxenon to reach the water surface is via steam bubbles.

## **3.4 The analysis procedure**

### **3.4.1 General**

This section gives a short description of the analysis procedure that is applied after the raw data is obtained from the beta-gamma coincidence set-up. It is implemented in analyzing software programs such as “bganalyze”, the software used at the CTBTO, or “XECON”, the FOI software. This method, as it is presented here, requires the assumption that we will not be dealing with extraordinarily low count rates, so the approximation from Binomial to Poisson distribution is justified.

All methods and calculations, that are described in this section, are found in [De Geer, 2007] if not stated otherwise. In the following formulae, all stochastic variables are assigned a color according to the statistics they follow: Red stands for Poisson distributed, blue for Gaussian distributed variables. Black stochastic variables are used for their true means or estimated (by measurement) true means. Constants are represented by black symbols.

### **3.4.2 The Net Count Calculation (NCC) method**

To relate the measured counts to a certain isotope, regions of interest (ROI) within the two-dimensional spectrum are defined. The net count value is then



obtained after a subtraction of background radiation and the interference of other nuclides. The ambient background is measured to quantify the natural radiation background of the particular detector set-up. It can vary depending on natural conditions like elevation above sea level. Interference counts are caused by daughter products of  $^{222}\text{Rn}$ , which could be contaminating the sample, or other radionuclides.

$^{222}\text{Rn}$  has a half-life of 3.8 d, long enough to survive the processing time. While  $^{222}\text{Rn}$  itself is an alpha emitter, its daughter nuclides  $^{214}\text{Bi}$  ( $T_{1/2} = 19.9$  m) and  $^{214}\text{Pb}$  ( $T_{1/2} = 26.8$  m) emit betas coincident with gamma radiation. They will, therefore, be seen in the beta-gamma spectrum. Because of their short half-lives they are in equilibrium with  $^{222}\text{Rn}$ , so the quantification of one daughter nuclide can be used to calculate the total radon contamination.

This is done via the 351,9 keV ( $I = 35.6\%$ ) gamma from an isomeric state of  $^{214}\text{Bi}$  in the decay of  $^{214}\text{Pb}$ . Because of its short half-life of less than 0.1 ns it delivers a signal coincident with the beta signal. The presence of  $^{222}\text{Rn}$  has an impact on all radionuclide ROIs. However, by knowing the total amount of  $^{222}\text{Rn}$  all interferences can be subtracted from the 2D array.

Interference is caused also by Compton scattering and X-rays from other radionuclides. It is clear that there is only interference from higher to lower gamma energies.

Additionally, the “memory effect” contributes possible interference: traces of radionuclides from a previous sample might still be present in the detector cell. Xenon as well as radon are able to diffuse into the walls of the scintillation cell and stay there even after the vial had been flushed and evacuated. Hence a gas background measurement is taken before every sample to correct for the memory effect.

In summary, the calculation of the net counts can be expressed [Saey and De Geer, 2007]:

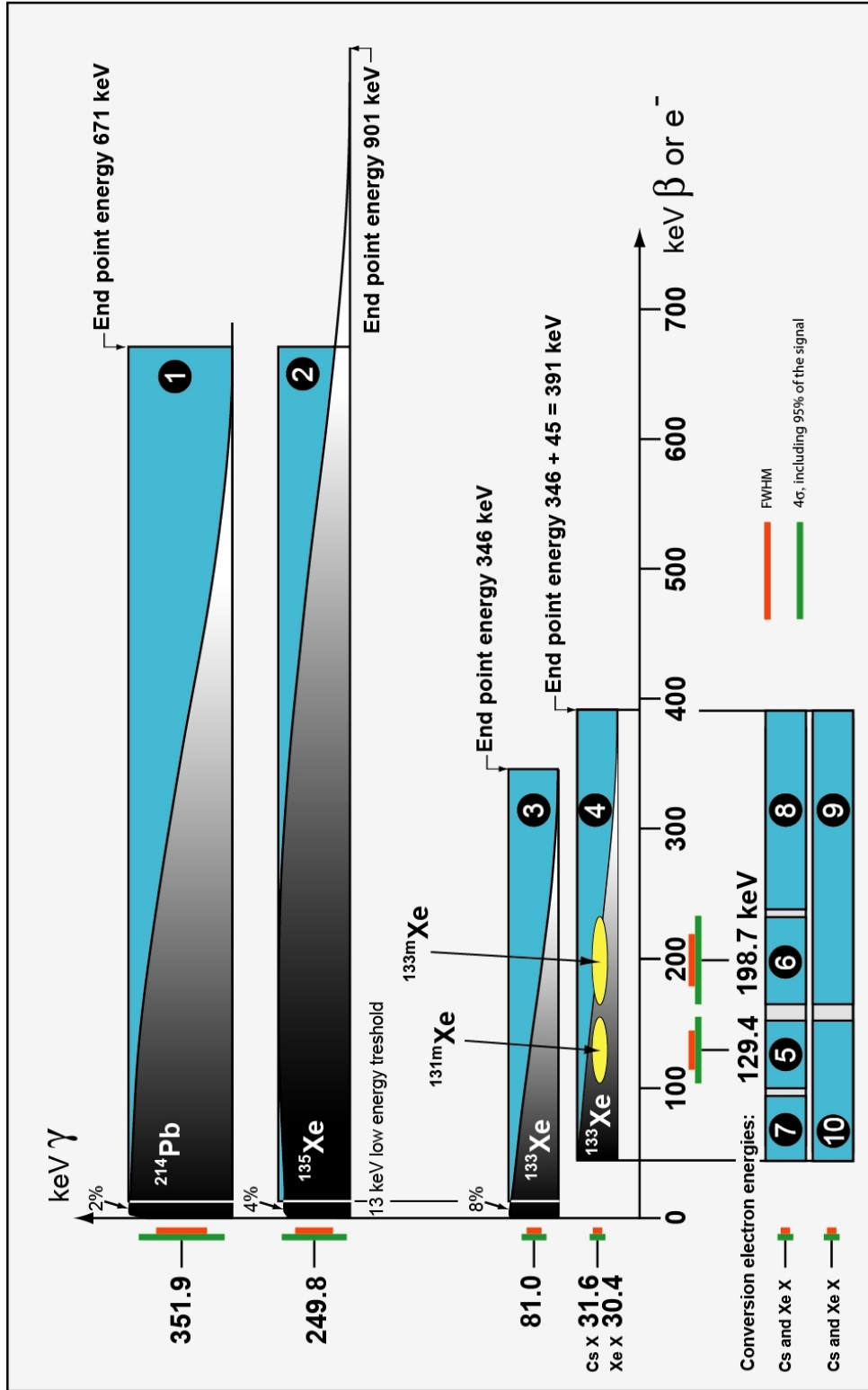


Figure 3.4: The 10 regions of interest in a two dimensional beta-gamma coincidence spectrum. Picture taken from [De Geer, 2007]

ROI Counts
minus Ambient Background
minus Interference from $^{222}\text{Rn}$
minus Interference from other radionuclides
minus Decay corrected Memory Effect
Net Counts

To quantify the effect of interference, factors of the form  $R_{i/j}$  are introduced:  $R_{i/j}$  is defined as the ratio between the counts in ROI  $i$  and the counts in ROI  $j$  for a sample, in which only the nuclide of ROI  $j$  is present. Interferences can only originate from the ROIs  $j=1$  ( $^{214}\text{Pb}$ ),  $j=2$  ( $^{135}\text{Xe}$ ) and  $j=3$  ( $^{133}\text{Xe}$ , 81 keV). In general, they include both Compton scattering from primary radiation and possible primary radiation of the owner nuclide of ROI  $j$  within the ROI  $i$ . These factors are determined in the initial calibration process. Note that all  $R_{i/j}$  factors vanish for  $i \leq j$  as there is no interference from lower to higher gamma energies.  $R_{i/j}$  is set to zero if the activity concentration of the interfering nuclide (the owner nuclide of ROI  $j$ ) is determined to lie below the critical level  $L_C$ . The  $L_C$  gives a value for the activity concentration under which the nuclide is treated as “not present”. The calculation of  $L_C$  will be described in detail in section 3.4.3.

Thus, the signal in ROI  $i$  can be calculated for the gas background and the sample with the general expressions:

$$\begin{aligned}
d_i &= [D_i - R_{i/1}D_1 - R_{i/2}D_2 - R_{i/3}D_3] - k_g[B_i - R_{i/1}B_1 - R_{i/2}B_2 - R_{i/3}B_3] \\
c_i &= [C_i - R_{i/1}C_1 - R_{i/2}C_2 - R_{i/3}C_3] - k_s[B_i - R_{i/1}B_1 - R_{i/2}B_2 - R_{i/3}B_3]
\end{aligned}$$

$d_i$	...	the signal in the gas background corrected for ambient background and interferences
$c_i$	...	the signal in the sample corrected for ambient background and interferences
$D_i$	...	the gross signal in ROI i in the gas background
$C_i$	...	the gross signal in ROI i in the sample
$B_i$	...	the signal in ROI i in the detector background, i.e the ambient background
$R_{i/j}$	...	the interference contribution of ROI i into ROI j
$k_g$	...	the ratio of the live counting time of the gas background divided by the live counting time of the detector background
$k_s$	...	the ratio of the live counting time of the gas background divided by the live counting time of the sample background

In the next step the net count value can be obtained by subtracting the signal in the gas background corrected for radioactive decay from the signal in the sample:

$$n_i = c_i - F_i d_i \quad (3.7)$$

$n_i$  ... the net count value for ROI i

$F_i$  ... the decay correction factor

Without a derivation (can be found in appendix 1 of [De Geer, 2007]), the decay correction factor  $F_i$  is given as:

$$F_i = \frac{t_{cL} t_{dR}}{t_{cR} t_{dL}} e^{-\lambda_i \tau} \frac{1 - e^{-\lambda_i t_c R}}{1 - e^{-\lambda_i t_d R}} \quad (3.8)$$

- $\lambda_i$  ... decay constant for owner nuclide of ROI i
- $\tau$  ... time between the beginning of the gas background measurement and the sample measurement
- $t_{cR}$  ... real time between the beginning of the sample measurement and the end of the sample measurement
- $t_{cL}$  ... live time between the beginning of the sample measurement and the end of the sample measurement
- $t_{dR}$  ... real time between the beginning of the gas background measurement and the end of the gas background measurement
- $t_{dL}$  ... live time between the beginning of the gas background measurement and the end of the gas background measurement

Which leads us to the explicit expression of the net count value:

$$\begin{aligned}
 n_i = & \textcolor{blue}{C}_i - R_{i/1}\textcolor{red}{C}_1 - R_{i/2}\textcolor{red}{C}_2 - R_{i/3}\textcolor{red}{C}_3 - F_i\textcolor{red}{D}_i + F_iR_{i/1}\textcolor{red}{D}_1 + F_iR_{i/2}\textcolor{red}{D}_2 \\
 & + F_iR_{i/3}\textcolor{red}{D}_3 - (k_s - F_ik_g)\textcolor{red}{B}_i + (k_sR_{i/1} - F_ik_gR_{i/1})\textcolor{red}{B}_1 \\
 & + (k_sR_{i/2} - F_ik_gR_{i/2})\textcolor{red}{B}_2 + (k_sR_{i/3} - F_ik_gR_{i/3})\textcolor{red}{B}_3
 \end{aligned} \quad (3.9)$$

Consequently, the activity concentration  $\textcolor{blue}{AC}_i$  is calculated by multiplying the net count value by a correction factor  $H_i$ , that includes detector efficiency, the branching ratio and radioactive decay during processing.

$$\textcolor{blue}{AC}_i = H_i n_i \quad (3.10)$$

with:

$$H_i = \frac{t_{cR}t_S}{t_{cL}} \cdot \frac{\lambda_i^2}{I_i V (1 - e^{-\lambda_i t_S}) e^{-\lambda_i t_P} (1 - e^{-\lambda_i t_{cR}})} Bq/m^3 \quad (3.11)$$

$\lambda_i$	...	decay constant for owner nuclide of ROI i
$t_{cR}$	...	real time between the beginning of the sample measurement and the end of the sample measurement
$t_{cL}$	...	live time between the beginning of the sample measurement and the end of the sample measurement
$t_S$	...	sampling time
$t_P$	...	processing time
$I_i$	...	detector efficiency times the branching ratio of the ROI i
$V$	...	total sample air volume

Again the full derivation can be found in [De Geer, 2007]. From these linear expressions the expectation values  $E(n_i)$  and  $E(AC_i)$  can be obtained by simply replacing all stochastic variables by their estimated true mean, which corresponds to the measured value (red changes to black):

$$\begin{aligned}
E(n_i) = & C_i - R_{i/1}C_1 - R_{i/2}C_2 - R_{i/3}C_3 - F_iD_i + F_iR_{i/1}D_1 + F_iR_{i/2}D_2 \\
& + F_iR_{i/3}D_3 - (k_s - F_ik_g)B_i + (k_sR_{i/1} - F_ik_gR_{i/1})B_1 \\
& + (k_sR_{i/2} - F_ik_gR_{i/2})B_2 + (k_sR_{i/3} - F_ik_gR_{i/3})B_3
\end{aligned} \tag{3.12}$$

and

$$E(AC_i) = H_iE(n_i) \tag{3.13}$$

The Variances  $V(n_i)$  and  $V(AC_i)$  are calculated using a general expression that holds for any two independent stochastic variables  $A$  and  $B$ :

$$V(aA \pm bB) = a^2V(A) + b^2V(B)$$

In case of Poisson variables,  $V(A)$  is estimated by  $A$  and  $V(B)$  is estimated by  $B$ , leading to:

$$V(aA \pm bB) = a^2A + b^2B$$

This holds for an arbitrary number of independent variables. This leads to:

$$\begin{aligned}
V(\mathbf{n}_i) = & C_i - R_{i/1}^2 C_1 - R_{i/2}^2 C_2 - R_{i/3}^2 C_3 - F_i^2 D_i + F_i^2 R_{i/1}^2 D_1 + F_i^2 R_{i/2}^2 D_2 \\
& + F_i^2 R_{i/3}^2 D_3 - (k_s - F_i k_g)^2 B_i + (k_s R_{i/1} - F_i k_g R_{i/1})^2 B_1 \\
& + (k_s R_{i/2} - F_i k_g R_{i/2})^2 B_2 + (k_s R_{i/3} - F_i k_g R_{i/3})^2 B_3
\end{aligned} \tag{3.14}$$

and

$$V(\mathbf{AC}_i) = H_i^2 V(\mathbf{n}_i) \tag{3.15}$$

### 3.4.3 Calculation of the Minimum Detectable Concentration

When analyzing an actual measurement it is important to be able to decide if a signal is present or not. Furthermore, the sensitivity of this decision needs to be quantified. Assuming a Gaussian process that produces a background count, it is difficult to determine if a substance was present and which risk is involved, when the measured gross count comes close to the true mean of the background.

In [Currie, 1968] Lloyd Currie describes a concept of detection limits in which he introduces a critical limit,  $L_C$ , and a detection limit,  $L_D$ . The concept requires the approximation from Binomial distribution to Poisson distribution and further to Gaussian distribution to hold.  $L_C$  is used to determine if a signal is present, it is calculated after the measurement.  $L_D$ , however, describes the measurement as such even before it is carried out [De Geer, 2004]. However, since we are dealing with probability distributions, these limits are inevitably related to risk. There is a probability to falsely decide that a substance is present, when in fact it is not (Type I error) and the probability to falsely determine a signal to be absent when in fact it is present (Type II error). In both cases a risk needs to be taken and it is common to apply the same risk to both types. This corresponds to a fractile  $k$  of the distribution. At e.g.  $k = 1.645$  the involved risk corresponds to 5%. Currie derived the expressions of  $L_C$  and  $L_D$  by using the characteristics of the Gaussian distribution:

$$L_C = k \sqrt{\mu \left(1 + \frac{1}{m}\right)} \tag{3.16}$$

$$L_D = k^2 + 2L_C \quad (3.17)$$

$\mu$  ... the true mean of the background signal  
 $m$  ... the number of background measurements  
 $k$  ... the fractile of the Gaussian distribution

The general expression for  $L_C$  can be simplified assuming a well known true mean of the background signal. This is justified by a detector background measurement which is by far longer than the sample measurements. Furthermore, in case of a Gaussian distribution  $\mu$  equals to the variance  $V_0$  ( $\sigma_0^2$ ). For all ROIs  $i$ , that gives:

$$L_{Ci} = k \sqrt{V_0(n_i)} \quad (3.18)$$

and

$$L_{Di} = k^2 + 2L_{Ci} \quad (3.19)$$

Now, on closer examination of the equations 3.12 and 3.14 it is clear that, when subtracting  $E(n_i)$  from  $V(n_i)$ ,  $C_i$  is being cancelled out. Thus, the difference is independent of the number of counts in the ROI  $i$ . Since it holds for all  $i$ , it also applies to the special case of  $E(n_i) = 0 \equiv E_0(n_i)$ , i.e. only background radiation counts.

This means:

$$V(n_i) - E(n_i) = V_0(n_i) - E_0(n_i) \quad (3.20)$$

and further:

$$V_0(n_i) = V(n_i) - E(n_i) \quad (3.21)$$



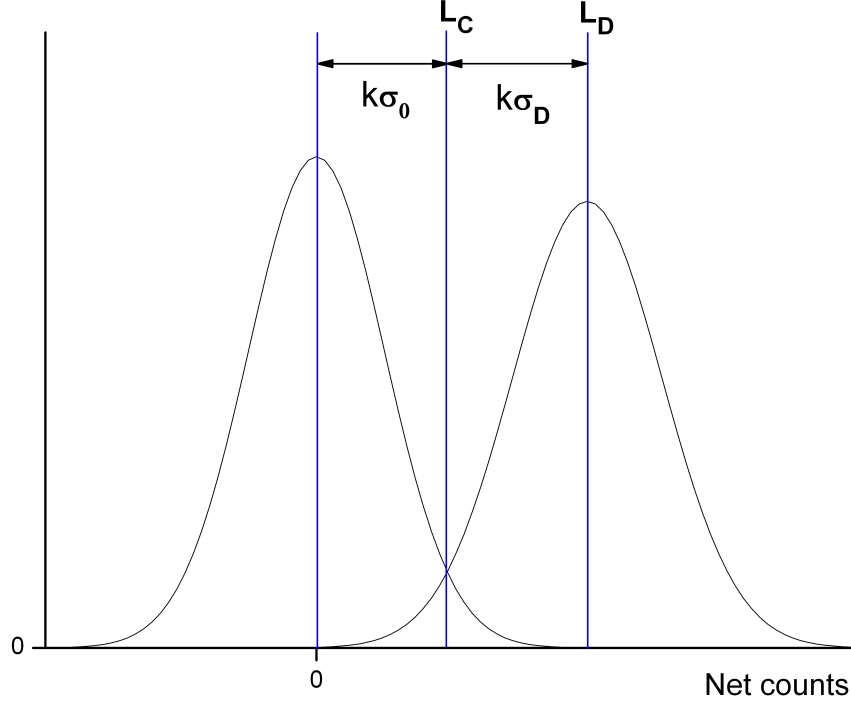


Figure 3.5: Two Gaussian distributions of net counts at true means of 0 and  $L_D$  with their corresponding standard derivations  $\sigma_0(= \sqrt{V_0})$  and  $\sigma_D(= \sqrt{V_D})$ .

Looking at figure 3.5 equation 3.18 becomes clear and equation 3.19 can be derived:

$$L_{Di} = L_{Ci} + k\sqrt{V_D(n_i)} = L_{Ci} + k\sqrt{V_0(n_i) + L_{Di}} \quad (3.22)$$

Where we used equation 3.20 for  $V_D(n_i) = V_0(n_i) + L_{Di}$ . Solving equation 3.22 gives equation 3.19.

Applying this on the derived values  $AC_i$  gives:

$$V(\textcolor{blue}{AC}_i) - H_i E(\textcolor{blue}{AC}_i) = V_0(\textcolor{blue}{AC}_i) - H_i E_0(\textcolor{blue}{AC}_i) \quad (3.23)$$

Now, the factor  $H_i$  has to be considered when we calculate the critical limit,  $L_{CACi}$ , and the detection limit,  $L_{DACi}$ , of the activity concentrations:

$$L_{CACi} = k\sqrt{V_0(\textcolor{blue}{n}_i)} \quad (3.24)$$

and

$$L_{DACi} = H_i k^2 + 2L_{CACi} \equiv MDC \quad (3.25)$$

$L_{DACi}$  is also called the Minimum Detectable Concentration, or MDC.

### 3.4.4 Corrections and revisions

During the short description of the analysis methods details were implicitly neglected and circumstances were simplified for the sake of a profound uncomplicated illustration of the theory. However, embracing these corrections increases the accuracy and correctness of the data analysis. It is not intended to present every correction and its derivation in detail, but to advise the reader of these issues. The interested reader can find all derivations in [De Geer, 2007].

- Growth correction for  $^{133m}\text{Xe} \rightarrow ^{133}\text{Xe}$

During transport, processing and sample measurement there is a continuous decay of  $^{133m}\text{Xe}$  into  $^{133}\text{Xe}$ . Thus, taking this feed into account, a corrective calculation for the activity concentration of  $^{133}\text{Xe}$  has to be performed both for the sample and the gas background. Note that this correction only affects  $^{133}\text{Xe}$ -ROIs, the calculation of the activity concentrations and the MDC.

- Merging data from different ROIs and the resulting covariances

In case of  $^{133}\text{Xe}$  several ROIs can be used to determine the total activity concentration (ROI 3,4,7,8,9,10). In any case the outcome will be more accurate using all possible information than using solely ROI 3. As long

as the measured concentrations of  $^{131m}\text{Xe}$  (ROI 5) and  $^{133m}\text{Xe}$  (ROI 6) stay below their critical limits, ROI 3 and ROI 4 are used. If, however, one or both metastable nuclides are measured above the critical limit, the ROIs 7 and 8 can be used to calculate the  $^{133}\text{Xe}$  activity concentration. The general solution in such a case is a weighted average of the activity concentrations, that minimizes the total variance:

$$V(AC_W) = \frac{\frac{AC_1}{V(AC_1)} + \frac{AC_2}{V(AC_2)}}{\frac{1}{V(AC_1)} + \frac{1}{V(AC_2)}} \quad (3.26)$$

Calculating  $V(AC_W)$ , a covariance term must be added, since the different channels are not statistically independent. This impacts the variances for  $^{133m}\text{Xe}$  but it has no effect on the expectation values.

- Covariance in the gas background

When the gas background ROIs are subtracted from the sample ROIs, covariances arise because both terms rely on the value (and the variance) of the detector background  $B_i$  at a given ROI  $i$ . In the description these terms were disregarded.

### 3.5 Classification of radioxenon samples

Many civilian facilities legally release radioxenon isotopes on a regular basis. It is of vital importance for the verification of compliance with the CTBT to be able to distinguish nuclear explosion scenarios from civilian sources. To support this, a number of methods for the characterization of radioxenon measurements are under investigation. In practice the data fusion with measurements from different technologies and a profound knowledge of the ambient radioxenon level are used to gain confidence about the origin of one sample. Nevertheless, there is a need for universal criteria applicable for radioxenon measurements and appropriate for source discrimination.

Single isotopic radioxenon activity ratios can help to differentiate between different sources, especially nuclear explosions from civil sources [Meyers, 1998], [Heimbigner et al., 2002]. The four radioxenon isotopes lead to six possible isotopic ratios, for reasons of simplicity the nuclide with the longer half-life as the denominator:  $^{135}\text{Xe}/^{133m}\text{Xe}$ ,  $^{135}\text{Xe}/^{133}\text{Xe}$ ,  $^{135}\text{Xe}/^{131m}\text{Xe}$ ,  $^{133m}\text{Xe}/^{133}\text{Xe}$ ,  $^{133m}\text{Xe}/^{131m}\text{Xe}$  and  $^{133}\text{Xe}/^{131m}\text{Xe}$ . Nuclear explosions yield isotopic ratios that are above typical reactor emissions. However, any initial ratio will change with time due to radioactive decay and follow an exponential decrease. This opens a time margin of a couple of days, during which a nuclear explosion can clearly be distinguished from reactor emissions. On the other hand, reactor emissions are never unambiguous, using only single isotopic ratios.

A robust method relying on the relationships of two different isotopic activity ratios was suggested in [Kalinowski et al., 2010]. The method requires two conditions, the detection of at least three different radioxenon isotopes and one single source as origin of these isotopes. It uses a set of plots that represent the relation of one isotopic activity ratio to another for analysis. Each plot is divided into two regions, the civil and the explosion domain, by a separation line. While the exact position of the separation line is still under investigation, first approximations are found in [Kalinowski et al., 2010]. A main advantage of this method is its independence from radioactive decay. Any combination of isotopic ratios will move along the separation line without crossing it.

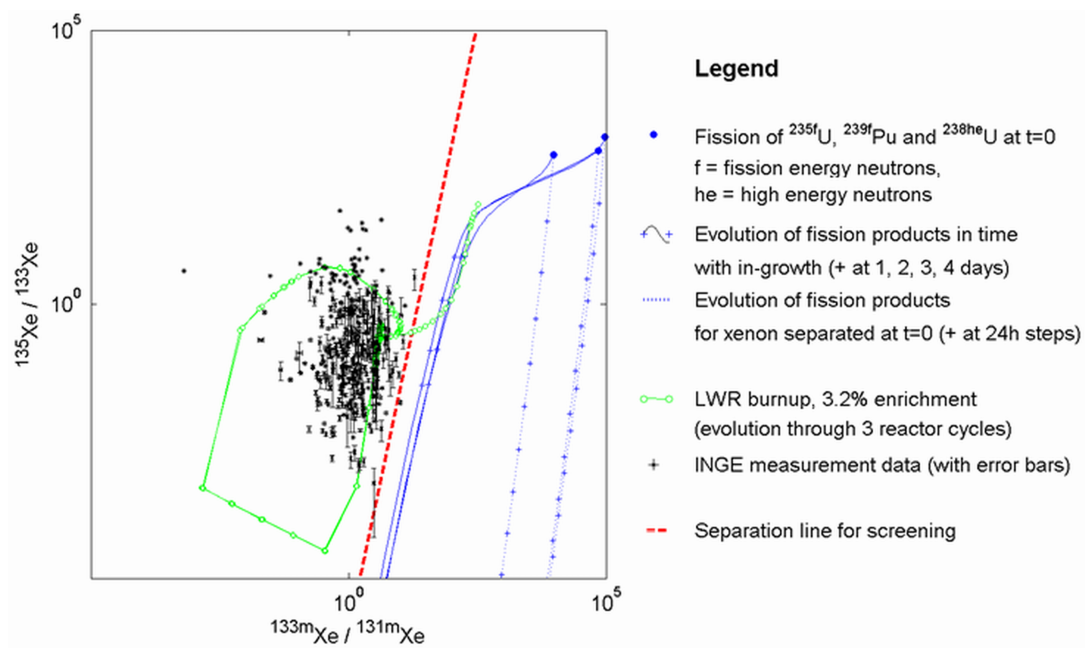


Figure 3.6: Source discrimination plot containing data of INGE measurements, calculated isotopic ratios typical for a nuclear explosion as well as emissions calculated for a light water reactor. Picture taken from [Kalinowski et al., 2010]

## 4 The measurement campaigns at the TRIGA reactor in Vienna

### 4.1 Experimental schedule and setup

Two campaigns of measurements were carried out during the time from 25 May until 29 May 2009 and from 27 October until 3 November with a SAUNA sampler. The transport columns were sent to the lab of the Swedish Defence Research Agency (FOI) in Stockholm for radionuclide analysis. The experimental schedule of both campaigns included following experiments:

- The background sample: After one weekend without reactor operation, this is the first sample taken.
- A sample during normal reactor operation: While the reactor is at a constant power of  $250 \text{ kW}_{\text{th}}$ , the air above the water surface of the reactor is sampled.
- A sample during reactor operation without active cooling: While the reactor operates at a constant power output of  $250 \text{ kW}_{\text{th}}$ , the active cooling circuit of the water is shut down.
- Irradiated air from five irradiation tubes: After a definite time span of reactor operation, the air inside of five irradiation tubes is sampled.
- Irradiation of a target containing HEU (93%  $^{235}\text{U}$ ) (total weight:  $240.2 \mu\text{g}$  HEU): With an Uranium target in one irradiation tube and the reactor at full power, nitrogen gas flushes the target and is sampled.

- Irradiation of a target containing HEU (93%  $^{235}\text{U}$ ) with a cadmium shielding (this experiment was only performed during the second campaign; total weight of target:  $237.7\text{ }\mu\text{g HEU}$ ): Cd-113, which occurs in natural cadmium at an abundance of 12.22%, has a neutron absorption cross section of 20647 b at 0.025 eV [KAERI, 2010]. Thus, natural cadmium provides efficient shielding from thermal neutrons and only epithermal and fast neutrons can reach the target and induce fission.

In preparation of the experiments a plastic foil was taped down to the ground of the reactor platform including the handrail around the reactor pool. Its purpose is to prohibit the air above the reactor surface to mix with the air in the reactor hall. However, it was not tried to build up a completely airtight boundary. In fact, the air intake of the SAUNA system requires an airflow into the “plastic tent”. Between the water surface and the reactor platform, there are a few gaps, through which air can flow. By letting these gaps open, a circulation of air is established during sampling.

The active water cooling of the reactor is provided by a spray of cool water at approximately half the height of the water tank. It establishes two circular water currents, one warm current around the core of the reactor and one cool current above. Besides active cooling, its main purpose is to slow down the rise of radioactive nuclides, mainly  $^{16}\text{N}$  ( $T_{1/2} = 7.13\text{ s}$ ), which is being produced in  $^{16}\text{O}(\text{n,p})^{16}\text{N}$  reactions in the water close to the reactor core during operation [Steinhauser, 2009].



Figure 4.1: Two photos of the reactor platform: The first one without the plastic tent and the second one with the plastic tent and the SAUNA sampler in the background.





Figure 4.2: A picture of one uranium target placed inside a hose. The smaller hose carrying the nitrogen inflow is not visible.

The uranium targets originate from old fission chambers and are composed of highly enriched uranium (93% HEU). A target is placed at one end of a hose, that has been closed tightly. Another hose of smaller diameter is added inside the first hose and connected with a nitrogen gas bottle. The wider hose leads to the SAUNA field sampler. This way, the nitrogen gas can pick up volatile fission products from the target, while it is irradiated, and transport them to the SAUNA system.

In the last experiment the effect of induced fission by unmoderated neutrons is investigated. Cadmium has a very high cross section for thermal neutrons and is therefore used as a filter for thermal neutrons. For this experiment the uranium target was fully surrounded by a 2 mm cadmium coating.

Although initially only one campaign was planned, a number of problems arose during and after the execution of the experiments that eventually led to the wish to re-run the experiments [Henriksson, 2009]. One problem was a high concentration of carbon dioxide in the samples. Carbon dioxide is believed to adsorb to activated charcoal and, in high concentrations, is able to occupy areas of the active surface decreasing the overall xenon sampling efficiency. Thus, for most samples it was not possible to quantify the total radioxenon amount that was sampled in the gas chromatograph. Further, due to unexpected unavailability of the detector in Freiburg (Germany), the samples had to be measured on a non-calibrated detector in Kista (Sweden).

## **4.2 Processing and analysis of the samples**

### **4.2.1 First experimental campaign**

The gas chromatograms of the experiments of the first campaign were very difficult to interpret, probably due to CO<sub>2</sub> saturation. The amount of xenon could, therefore, not be determined for all the samples. In addition an error occurred during the transfer of the samples 2, 4 and 6, so that the amount of xenon remained unclear. The samples 3, 5, and 8 were severely affected by CO<sub>2</sub> saturation, which made a volume estimation impossible. Sample 7 was measured after sample 9, which was rather strong in activity, and suffered from memory effects. The only samples suitable to obtain reasonable data from this first campaign were samples 1 and 9.

	Air vol. [m <sup>3</sup> ]	Expected Xe vol. [ml]	Sampled Xe vol. [ml]	Yield [%]	Operation mode
1	9.1	0.80	0.26	33	Background
2	7.9	0.69	n/a	n/a	250kW; active cooling
3	17.9	1.57	n/a	n/a	250kW; active cooling
4	7.1	0.62	n/a	n/a	250kW; without active cooling
5	17.8	1.55	n/a	n/a	250kW; active cooling
6	6.9	0.60	n/a	n/a	250kW; active cooling
7	17.5	1.53	n/a	n/a	250kW; active cooling
8	0.080	0.0070	n/a	n/a	Irradiation tubes
9	0.072	0.0063	0.09	1429	Irradiation of HEU target

Table 4.1: The experiments of the first campaign. Data taken from [Ringbom et al., 2009]

Sample 1 shows a fairly low sampling yield, probably due to problems during sample transfer into the transport column. On the other hand sample 9 has an extremely large yield. The very small amount of xenon in sample 9 is believed to result in an inaccurate quantification in the gas chromatograph. More importantly, nitrogen was used as a carrier gas from the uranium target to the SAUNA system, which makes the total amount of xenon hard to estimate.

#### 4.2.2 Second experimental campaign

Prior to the second campaign the detector system SEL01 in Kista was properly calibrated with respect to energy and efficiency. Because of the CO<sub>2</sub> problem during the first campaign, an additional CO<sub>2</sub> remover including a basic solution was placed in front of the intake air duct for the samples 4 and 5. CO<sub>2</sub> as an acidic gas can be absorbed flowing through a basic solution, for which NaOH was used. Moreover, one extra water filter was inserted for all samples.

	Air vol. [m <sup>3</sup> ]	Expected Xe vol.(STP) [ml]	Sampled Xe vol. [ml]	Yield [%]	Operation mode
1	9.98	0.79	0.002	0.3	Background
2	5.77	0.45	0.042	9	250kW; active cooling
3	1.23	0.10	0.105	105	250kW; without active cooling
4	5.71	0.45	0.5	111	250kW; active cooling; extra CO <sub>2</sub> remover
5	1.24	0.10	0.104	104	250kW; without active cooling; CO <sub>2</sub> remover
6	0.19	0.015	0.03	200	Irradiation tubes
7	0.44	0.035	0.008	23	Irradiated HEU target
8	0.38	0.03	0.003	10	Irradiated HEU target; cadmium shielding
9	2.94	0.23	0.25	109	Background
10	3.01	0.24	0.26	108	250kW; active cooling

Table 4.2: The experiments of the second campaign. Data were taken from [Ringbom et al., 2009]

The sampling of the background failed because of untight hoses within the helium supply, sample 1 is therefore not useful for analysis. Sample 2 shows a rather low xenon yield, the reasons for this are not fully understood until now. Sample 6 has a yield far above 100%, likely due to the same reasons as in sample 9 of the first campaign. Number 7 and 8 were again sampled with nitrogen carrier gas, which results in a vague calculated quantity of xenon. The remaining samples show yields between 104% and 111%. The reason for this is probably found in an imprecision in the calibration of the gas chromatograph [Ringbom et al., 2009].

### 4.3 Results and discussions

The results of both campaigns are given in table 4.3. Dark gray cell colors mark concentrations below the critical limit  $L_C$ . However, since the detector system SEL01 in Kista was not calibrated for efficiency, the efficiency calibration of a different SAUNA detector was used the samples of the first campaign are afflicted with an additional 20% of systematic uncertainties [Ringbom et al., 2009]. Also, in case of the HEU samples additional systematic uncertainties are probable due to the small sampling volumes. Nevertheless, systematic uncertainties should cancel out to a large degree, when isotopic ratios are calculated.

The measured  $^{133}\text{Xe}$  activity concentrations were found between 11 Bq/m<sup>3</sup> to 70 Bq/m<sup>3</sup> for normal reactor operation at full power. The samples contained  $^{131m}\text{Xe}$  varying from 0.01 Bq/m<sup>3</sup> to 0.8 Bq/m<sup>3</sup> and activity concentrations between 0.06 Bq/m<sup>3</sup> and 14 Bq/m<sup>3</sup> for  $^{133m}\text{Xe}$ . Despite the long transport times from Austria to Sweden,  $^{135}\text{Xe}$ , which has a half-life of 9.1 h, was possible to detect in six samples at concentrations between 29 Bq/m<sup>3</sup> and  $1.6 \times 10^4$  Bq/m<sup>3</sup>.

	Xe-131m $[[\text{Bq}/\text{m}^3]]$			Xe-133m $[\text{Bq}/\text{m}^3]$		
Sample	Act. Conc.	$\sigma$	LC	MDC	Act. Conc.	MDC
<b>Campaign 1</b>						
1	1.08E-02	4.39E-03	7.16E-03	n/a	5.81E-02	1.81E-02
9	1.25E-01	7.39E-02	1.20E-01	n/a	4.82E+00	5.07E-01
<b>Campaign 2</b>						
2	8.47E-01	6.75E-02	1.09E-01	n/a	2.47E+00	9.64E-02
3	1.81E-01	1.94E-02	3.14E-02	n/a	4.97E-01	2.80E-02
4	1.65E-01	7.61E-03	1.23E-02	n/a	7.13E-01	2.58E-02
5	1.67E-01	2.25E-02	3.66E-02	n/a	7.13E-01	9.26E-02
6	6.64E-01	4.11E-02	6.48E-02	n/a	3.45E+00	8.83E-02
7	2.40E-01	1.31E-01	2.03E-01	n/a	1.40E+01	2.93E-01
8	4.01E-01	4.42E-01	7.26E-01	1.46E+00	3.29E+00	2.15E+00
9	3.86E-02	7.34E-03	1.19E-02	n/a	3.20E-01	3.98E-02
10	1.04E-01	1.06E-02	1.72E-02	n/a	5.94E-01	5.95E-02
<b>Xe-135 <math>[[\text{Bq}/\text{m}^3]]</math></b>						
Sample	Act. Conc.	$\sigma$	LC	MDC	Act. Conc.	MDC
<b>Campaign 1</b>						
1	1.58E+00	9.60E-03	7.62E-03	n/a	2.33E-02	2.86E-02
9	9.54E+00	1.81E-01	1.63E-01	n/a	7.42E+03	5.17E+02
<b>Campaign 2</b>						
2	6.69E+01	1.21E-01	3.62E-02	n/a	1.37E+02	8.14E-01
3	1.58E+01	3.48E-02	2.49E-02	n/a	2.91E+01	2.32E-01
4	1.41E+01	1.93E-02	1.48E-02	n/a	5.90E+01	4.21E+00
5	1.15E+01	6.18E-02	8.25E-02	n/a	5.64E+01	7.18E+01
6	1.76E+01	8.08E-02	7.29E-02	n/a	1.89E+02	3.79E+00
7	3.31E+01	4.39E-01	1.20E+00	n/a	1.62E+04	3.00E-02
8	1.83E+01	1.22E+00	1.97E+00	n/a	9.02E+02	1.08E+04
9	5.92E+00	2.39E-02	2.55E-02	n/a	1.41E+02	1.41E+02
10	1.34E+01	3.54E-02	3.70E-02	n/a	1.51E+02	1.74E+02

Table 4.3: The results from the activity concentration analysis. Data were taken from [Ringbom et al., 2009]

Some samples of the second campaign are found to contain counts originating from  $^{125}\text{Xe}$ , which does not belong to the CTBT-relevant nuclides. Xenon-125 has a half-life of about 16.9 h and decays to  $^{125}\text{I}$  via almost 100% electron capture [ENSDF, 2009]. Gamma energies, interesting for analysis are: 243 keV (30.1%), 188 keV (54.0%) and 55 keV (6.8%). Conversion electrons are found at: 210 keV (1.9%), 155 keV (6.3%) and 22 keV (24.8%) together with X-ray energies around 30 keV. Within the beta-gamma spectrum  $^{125}\text{Xe}$  is mostly visible through its 22 keV (24.8%) conversion electron detected in coincidence with a X-ray photon (30 keV) and/or any other possible gamma photon originating from a different  $^{125}\text{Xe}$ -decay. A rough estimation was made analysing sample 6, which had the largest amount of  $^{125}\text{Xe}$ , resulting in an activity concentration of 170 Bq/m<sup>3</sup> [Ringbom et al., 2009]. Figure 4.3, which is based on numerical simulations, shows an approximate  $^{125}\text{Xe}/^{133}\text{Xe}$  ratio of 10:1, which fits to the measured  $^{133}\text{Xe}$  activity concentration of 17.6 Bq/m<sup>3</sup> (see table 4.3). The impact of  $^{125}\text{Xe}$  on the measured activity concentration of  $^{135}\text{Xe}$  was minimized by redefining the  $^{125}\text{Xe}$ -ROI and its overall efficiency.

The isotopic ratios of all measurements, in which the four CTBT-relevant radioxenon isotopes were detected, lie on the civil side of the discrimination line. These are the samples 2,3,4,6 and 7 of the second campaign and the sample 9 of the first campaign. Together with a background sample (no. 9 of the second campaign), in which, since no  $^{135}\text{Xe}$  was detected, the MDC was used as its  $^{135}\text{Xe}$ -activity concentration, their isotopic ratios can be seen in figure 4.4.

Looking at the four-nuclide plot, the reactor air samples are found in the civil region as expected. Also, the activity ratios of the sample containing irradiated air are in line with the simulation. The measurements of the HEU targets, however, are shifted to the left, far from theoretical predictions. The black solid line symbolizes the time evolution of the activity ratios for samples that suffer full in-growth from parent nuclides, while the black dashed line shows the decay after the radioxenon isotopes have been separated from their precursors. This was done after ten minutes of nitrogen flushing.

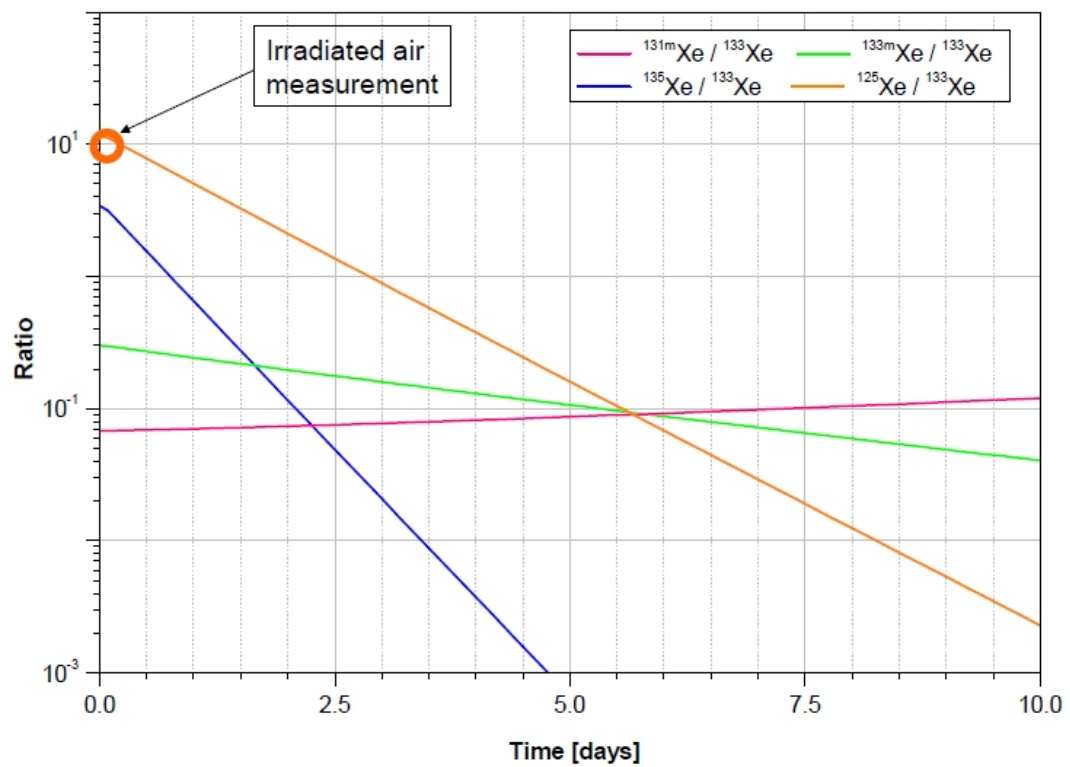


Figure 4.3: Simulations on the time evolution of some activity ratios, especially  $^{125}\text{Xe}/^{133}\text{Xe}$ . The sampling was finished within ten minutes [Saey, 2010a].



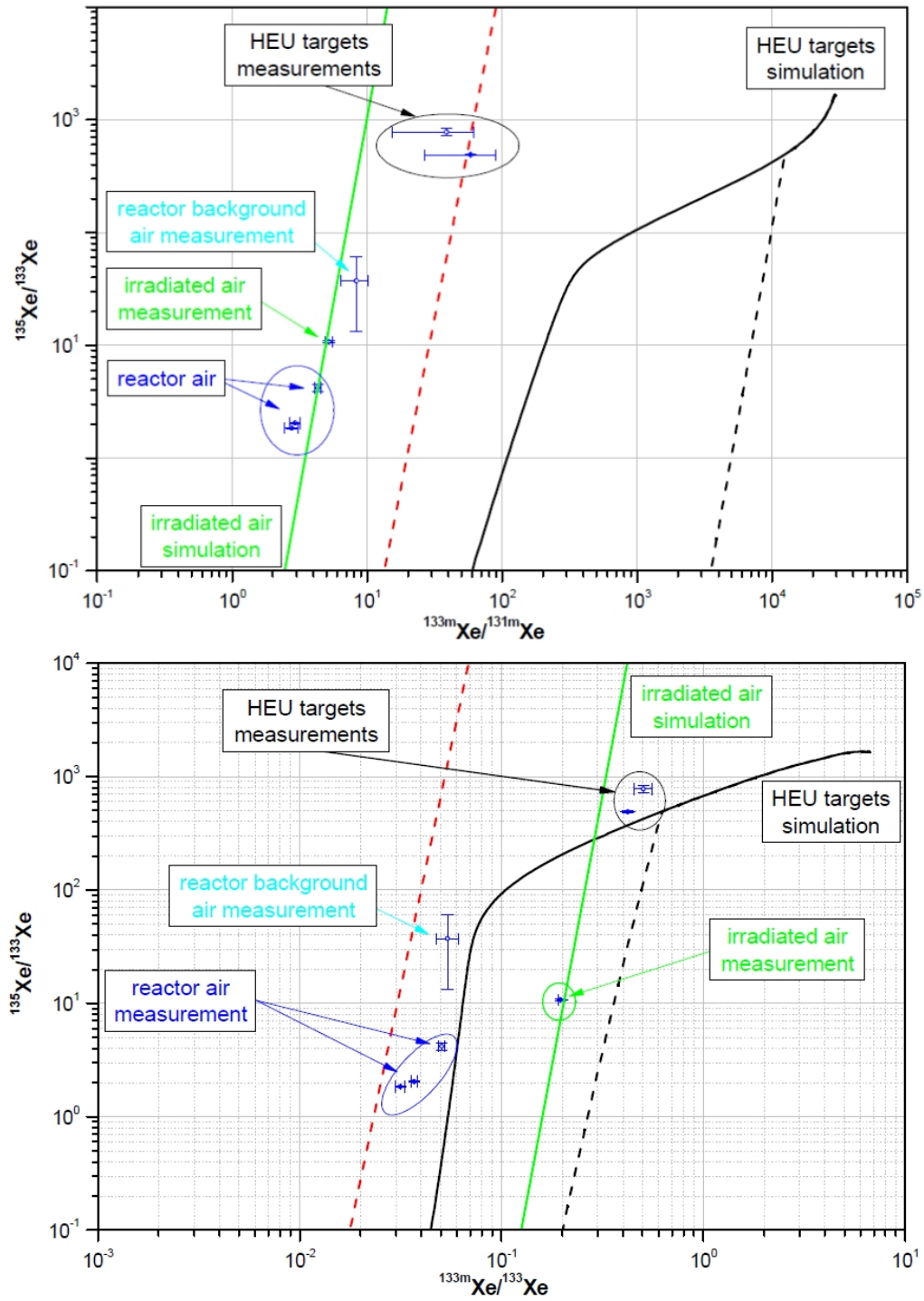


Figure 4.4: Data of the measurements and numerical calculations in a four-radionuclide plot (above) and a three-radionuclide plot (below). The red dashed line is the discrimination line dividing the plots into a nuclear power plant region (left) and a explosion scenario region (right) [Saey, 2010a].

In the three-nuclide plot, which disregards the  $^{131m}\text{Xe}$  activity concentrations, the HEU samples fit much better to the simulations. The reason for this, however, is not fully understood for the time being. The data of the remaining samples, although they are all found on the right-hand side of the discrimination line, do not stand in contrast to the four-nuclide plot (see [Kalinowski et al., 2010] for more information).

## 5 Conclusions and outlook

Prior to the experiments it was unclear which activity concentrations of radioxenon releases were to expect from a typical research reactor. Estimations have been made that resulted in activity concentrations ranging from 0.7 GBq/m<sup>3</sup> in the event of a total cladding failure of one fuel element to concentrations too low for measurement ( $< 1$  mBq/m<sup>3</sup>). The experiments explicitly show the presence of all four CTBT-relevant radioxenon isotopes plus <sup>125</sup>Xe, especially in the sample containing activated air from the irradiation tubes.

The samples containing all four CTBT-relevant radioxenon isotopes are found to be in the civil area following the screening criteria proposed in [Kalinowski et al., 2010]. This also holds for the two samples that were taken from irradiated HEU targets.

With exception of <sup>125</sup>Xe, which is being produced by neutron capture of environmental <sup>124</sup>Xe, the origin of the radioxenon isotopes could not be clarified. Accounting for a 10% overall xenon transport efficiency, estimations regarding a complete fuel element failure would still result in activity concentrations at least six orders of magnitude stronger. The radioxenon could, however, stem from a pin hole or a hairline crack which releases only a minor percentage of the gaseous fission product inventory. Matters are similar focusing on the uranium contamination of the outside of the fuel element claddings, where estimations yield activity concentrations of about the same order of magnitude. In this case it seems reasonable, that the initial amount of <sup>235</sup>U has drastically decreased over time due to dissolving into the reactor water, which is continuously cleaned by an ion exchanger.

However, the explicit identification of the true origin(s) of the measured ra-

dioxenon isotopes remains unclear and evidences the necessity of further studies.

## 6 Epilogue

On February 9, literally at the final stage of this work, during a routine inspection of the fuel elements (fuel element length measurements) and the SAUNA sampler being dismantled already, one fuel element was found to be stuck in its core position. From the area around this fuel element the release of gas bubbles was observed, some of which were caught by hand in a glass flask and analyzed by a conventional gamma detector. All four CTBT-relevant radioxenon isotopes were detected in the sample in the maximum range of kBq ( $^{133}\text{Xe}$ ), however, exact activity concentrations remain to be studied. It is most likely that this fuel element had a damaged cladding, and therefore is to be seen as the reason for the radioxenon emissions observed in this study. Further investigations are in progress.

In any case, the results presented in this work, especially the total numbers on the radioxenon amounts, have to be viewed under this aspect.

# Bibliography

- M. Auer, A. Axelsson, X. Blanchard, T. W. Bowyer, G. Brachet, I. Bulowski, Y. Dubasov, K. Elmgren, J. P. Fontaine, W. Harms, J. C. Hayes, T. R. Heim-bigner, J. I. McIntyre, M. E. Panisko, Y. Popov, A. Ringbom, H. Sartorius, S. Schmid, J. Schulze, C. Schlosser, T. Taffary, W. Weiss, and B. Wernsperger. Intercomparison experiments of systems for the measurement of xenon ra-dionuclides in the atmosphere. *Applied Radiation and Isotopes*, 60(6):863–877, Jun 2004.
- A. Axelsson. Development, demonstration, testing and evaluation of on-site in-spection equipment for xenon sampling, separation and measurement. Tech-nical report, CTBTO, 2007.
- H. Böck. Personal communication. Atominstitut Wien, November 2009.
- H. Böck, H. Gallhammer, J. Hammer, and M. Israr. A combined wet/dry sipping cell for investigating failed TRIGA fuel elements. *AIAU 87310*, 1987.
- J. Bernstein. *Nuclear Weapons*. Cambridge University Press, 2008.
- CRC. *Handbook of Chemistry and Physics*. Chemical Rubber Company Press, 67th edition edition, 1987.
- L. Currie. Limits for qualitative detection and quantitative determination: ap-plication to radiochemistry. *Analytical Chemistry*, 40:586–593, 1968.
- O. Dahlman, S. Mykkeltveit, and H. Haak. *Nuclear Test Ban*. Springer Sci-ence+Business Media B.V., 2009.

- L-E. De Geer. Atmospheric radionuclide monitoring: a Swedish perspective. *In: Monitoring a Comprehensive Nuclear Test Ban Treaty*, The Netherlands: Kluwer Academic Publishers:157–177, 1996.
- L-E. De Geer. Comprehensive Nuclear-Test-Ban-Treaty: relevant radionuclides. *Kerntechnik*, 66(3):113–120, 2001.
- L-E. De Geer. Currie detection limits in gamma-ray spectroscopy. *Applied Radiation and Isotopes*, 61(2-3):151–160, 2004. Low Level Radionuclide Measurement Techniques - ICRM.
- L-E. De Geer. The xenon NCC method revisited. Technical report, FOI, 2007.
- L-E. De Geer. Personal communication. FOI, Swedish Defence Research Agency, May 2009.
- D. Ehhalt, K. Muennich, W. Roether, J. Schoelch, and W. Stich. Artificially produced radioactive noble gases in the atmosphere. *Journal of Geophysical Research*, 68:3817–3821, 1963.
- T. England and B. Rider. Evaluation and compilation of fission product yields. *Los Alamos National Laboratory Report LA-UR-94-3106; ENDF-349*, 1994.
- ENSDF. Evaluated nuclear structure data file. Accessed: 12 December, 2009. URL <http://www.nndc.bnl.gov/ensdf>.
- D. Fouquet, J. Razvi, and W. Whittemore (General Atomics). TRIGA research reactors: A pathway to the peaceful applications of nuclear energy. *Nuclear News*, 46(2):46–56, 2003.
- S. Glasstone, editor. *The effects of nuclear weapons*. United States Department of Defense, 1977.
- T.R. Heimbigner, J.I. McIntyre, T.W. Bowyer, J.C. Hayes, and M.E. Panisko. Environmental monitoring of radioxenon in support of the radionuclide measurement system of the international monitoring system. *24th Seismic Re-*

- search Review - Nuclear Explosion Monitoring: Innovation and Integration*, 2002.
- H. Henriksson. Measurements on the Vienna TRIGA reactor 25-29 May 2009. *FOI Memo 120*, 2009.
- L. Hoddeson, P. Henriksen, R. Meade, and C. Westfall. *Critical Assembly*. Cambridge University Press, 1993.
- W. Hoffmann, R. Kebeasy, and P. Firbas. Introduction to the verification regime of the comprehensive nuclear-test-ban treaty. *Physics of the Earth and Planetary Interiors*, 113(1-4):5–9, 1999.
- KAERI. Korea atomic energy research institute. Accessed: 2 February, 2010. URL <http://atom.kaeri.re.kr/>.
- M. Kalinowski, A. Axelsson, M. Beanand, X. Blanchard, T. Bowyer, G. Brachet, J. McIntyre, C. Pistner, M. Raith, A. Ringbom, P. Saey, C. Schlosser, T. Stocki, T. Taffary, and R. Ungar. Discrimination of nuclear explosions against civilian sources based on atmospheric isotopic activity ratios. *Pure and Applied Geophysics*, 167(4-5), 2010.
- R. Khan. *Neutronics Analysis of TRIGA Mark II Research Reactor and its Facilities*. PhD thesis, TU Wien, 2010.
- Y. Khariton and Y. Smirnov. The Khariton version. *Bulletin of the Atomic Scientists*, 5:20–31, 1993.
- LANL. Los Alamos National Laboratory. Accessed: 28 October, 2009. URL [http://www.lanl.gov/history/atomicbomb/trinity\\_gallery](http://www.lanl.gov/history/atomicbomb/trinity_gallery).
- K. Lindh. Personal communication. FOI, Swedish Defence Research Agency, November 2009.
- A. Makhijani, H. Hu, and K. Yih, editors. *Nuclear Wastelands*. The MIT Press, 1995.



- K. Matthews and L.-E. De Geer. Processing of data from a global atmospheric radioactivity monitoring network for CTBT verification purposes. *Journal of Radioanalytical and Nuclear Chemistry*, 263:235–240, 2005.
- L. Meitner and O. Frisch. Disintegration of uranium by neutrons: A new type of nuclear reaction. *Nature*, 143:239–240, 1939.
- R. Meyers, editor. *Encyclopedia of Environmental Analysis and Remediation*. John Wiley and Sons, 1998.
- A. Oughterson and W. Shields, editors. *Medical effects of the atomic bomb in Japan*. McGraw-Hill Book Company, Inc., 1956.
- PRIS. Power reactor information service of the international atomic energy agency. Accessed: 17 October, 2009. URL <http://www.iaea.org/programmes/a2/>.
- P. Reeder, T. Bowyer, J. McIntyre, W. Pitts, A. Ringbom, and C. Johansson. Gain calibration of a beta-gamma coincidence spectrometer for automated radioxenon analysis. *Nuclear Instruments and Methods in Physics Research Section A: Accelerators, Spectrometers, Detectors and Associated Equipment*, 521(2-3):586–599, 2004.
- R. Rhodes. *Dark Sun: The Making of the Hydrogen Bomb*. Simon and Schuster, 1995.
- A. Ringbom, T. Larson, A. Axelsson, K. Elmgren, and C. Johansson. Sauna—a system for automatic sampling, processing, and analysis of radioactive xenon. *Nuclear Instruments and Methods in Physics Research Section A: Accelerators, Spectrometers, Detectors and Associated Equipment*, 508(3):542–553, 2003.
- A. Ringbom, P. Andersson, L.-E. De Geer, K. Elmgren, H. Henriksson, K. Lindh, and J. Peterson. Measurements of radioxenon in the Vienna TRIGA reactor. *FOI Memo 3010*, 2009.

- P. Saey. Ultra-low-level measurements of argon, krypton and radon for treaty verification purposes. *Esarda Bulletin*, 36:42–56, 2007.
- P. Saey. The influence of radiopharmaceutical isotope production on the global radon background. *Journal of Environmental Radioactivity*, 100(5):396–406, May 2009.
- P. Saey. Personal communication. IAEA, International Atomic Energy Agency, February 2010a.
- P. Saey and L-E. De Geer. Notes on radon measurements for CTBT verification purposes. *Applied Radiation and Isotopes*, 63(5-6):765–773, 2005.
- P. Saey and L-E. De Geer. Technical report on noble gas data processing in support of CTBT verification. Technical report, Provisional Technical Secretariat (PTS) for the CTBTO, 2007.
- P. Saey, , C. Schlosser, P. Achim, M. Auer, A. Axelsson, A. Becker, X. Blanchard, G. Brachet, L. Cella, L-E. De Geer, M. Kalinowski, G. Le Petit, J. Peterson, V. Popov, Y. Popov, A. Ringbom, H. Sartorius, T. Taffary, and M. Zähringer. Environmental radon levels in europe: A comprehensive overview. *Pure and Applied Geophysics*, 2010b.
- J. Schulze, M. Auer, and R. Werzi. Low level radioactivity measurement in support of the CTBTO. *Applied Radiation and Isotopes*, 53(1-2):23–30, 2000.
- G. Steinhauser. Personal communication. Atominstitut Wien, November 2009.
- H. Stockburger, H. Sartorius, and A. Sittkus. Messung der Krypton-85- und Xenon-133-Aktivität der atmosphärischen Luft. *Zeitschrift für Naturforschung*, 32a:1249–1253, 1977.
- D. Underhill. The adsorption of argon, krypton and xenon on activated charcoal. *Health Physics*, 71:160–166, 1996.
- UNGA. United Nations General Assembly resolution number 50/245. 1996.

- K. Winger, J. Feichter, M.B. Kalinowski, H. Sartorius, and C. Schlosser. A new compilation of the atmospheric Kr-85 inventories from 1945 to 2000 and its evaluation in a global transport model. *Journal of Environmental Radioactivity*, 80(2):183–215, 2005.
- J. Wolber, S. Doran, M. Leach, and A. Bifone. Measuring diffusion of xenon in solution with hyperpolarized Xe-129 NMR. *Chemical Physics Letters*, 296(3-4):391 – 396, 1998. ISSN 0009-2614.
- C. Ziegler and D. Jacobson. *Spying without spies: origins of America’s secret nuclear surveillance system*. Praeger, Westport, Conn., 1995.

# Acknowledgments

First and foremost I would like to thank Prof. Helmuth Böck for giving me the unique chance to work in such an interesting field of study and offering me great encouragement throughout the whole project.

I would like to extend my sincerest thanks to the members of the FOI for showing patience with me and providing outstanding help especially Per Andersson, Lars-Erik de Geer, Klas Elmgren, Hans Henriksson, Karin Lindh, Jenny Petersson and Anders Ringbom.

Furthermore I wish to thank Mario Villa and Rustam Khan of the Atominstitut Wien as well as Mika Nikkinen of the CTBTO for their valuable assistance and advice.

I owe deep gratitude to my science advisors and friends Paul Saey and Georg Steinhauser, who provided me with the best support one could wish for. They both have gone beyond making contributions to the work and have helped to greatly enrich my knowledge.

Special thanks goes to my family, especially my mother Monika, my girlfriend Elvira and all my friends.

I would like to express my appreciation to the CTBTO and the FOI for sponsoring the measurement campaigns.

# Curriculum Vitae

## Persönliches:

Name: Michael Lechermann  
Geboren am: 12.6.1983 in Klagenfurt  
Staatsbürgerschaft: Deutschland

## Ausbildung:

Seit 2008 Diplomarbeit am Atominstitut Wien  
2005 Praktikum am Paul Scherrer Institut in Villigen, Schweiz  
Seit 2002 Physikstudium an der Universität Wien  
2001 – 2002 Studium an der Montanuniversität Leoben  
2001 Matura  
1989 – 2001 Grundschule anschließend BG Tanzenberg